CDF/ANAL/HEAVYFLAVOR/CDFR/1975
Version 3.0
December 30, 1993

Top Dilepton Analysis

T. Chikamatsu[1], A. Martin[2], J. Romano[3], J. Wang[3], A. Beretvas[4], M. Contreras[3], L. Demortier[5], H. Frisch[3], S. Kopp[3], Y. Seiya[1], L. Song[4], L. Stanco[6], C. Wendt[7], Q. F. Wang[5], and G. P. Yeh[4]

[1] *University of Tsukuba,* [2] *University of Illinois,* [3] *University of Chicago,* [4] *Fermilab,* [5] *Rockefeller University,* [6] *INFN/Padova,* [7] *University of Wisconsin*

1 Introduction

A search for $t\bar{t} \rightarrow$ dilepton + X in $p\bar{p}$ collisions at $\sqrt{s} = 1.8$ TeV is described. The signature used in this analysis is two high-P_T leptons from $t\bar{t} \rightarrow W^+b\ W^-\ \bar{b} \rightarrow \ell_1\ell_2X$, where $\ell_{1,2} =$ e or μ. Both leptons must have $P_T > 20$ GeV/c for an event to be in our signal region. Most of the acceptance comes from leptons from a W-decay, but electrons and muons from b or τ-decay are also accepted. Additional kinematic and event topology cuts are applied to reject backgrounds. The two leptons must have opposite electric charges, and the missing transverse energy ($\not\!\!E_T$) must be greater than 25 GeV. For events with $\not\!\!E_T < 50$ GeV, we also require $\Delta\phi(\not\!\!E_T, \ell) > 20°$, and $\Delta\phi(\not\!\!E_T, j) > 20°$, where $\Delta\phi(\not\!\!E_T, \ell)$ is the azimuthal opening angle between the $\not\!\!E_T$ and the nearest lepton, and $\Delta\phi(\not\!\!E_T, j)$ is the azimuthal opening angle between the $\not\!\!E_T$ and the nearest jet. The Z^0 and Drell-Yan backgrounds are reduced further by a dilepton invariant mass ($M_{\ell\ell}$) cut around the Z^0 peak (75 GeV/c^2 < 105 GeV/c^2). Finally, we require each event to have two or more jets with uncorrected $E_T > 10$ GeV. Distributions of several reconstructed variables from Monte Carlo top events are shown in Figure 1, for $M_{top} = 140$ GeV sample with 6780 pb^{-1}. Unless otherwise stated, all our Monte Carlo samples were generated with Isajet v6.43 + QFL.

A lower limit of 85 GeV/c^2 on M_{top} was obtained from the dilepton channel alone using 4.1 pb^{-1} of data collected in 1988-1989. When combined with the results from the lepton + jets + b channel, where the b was tagged through its semileptonic decay into muons, the detection efficiency increased by about 30% and an improved limit of 91 GeV/c^2 at the 95% confidence level was obtained. These analyses are described in detail in [1].

In this note we present the dilepton analysis for the 21.4 pb^{-1} of data collected by CDF in the 1992-1993 run. The next section describes our data sample and the criteria used to select leptons in various detectors. Kinematical and topological cuts designed to enhance the signal to background ratio are discussed in section 3. Section 4 reviews the effect of these cuts on data. Some expert comments on the $t\bar{t}$ candidates observed in the current run are presented in section 5. Section 6 explains in detail the computation of the total detection efficiency. A study of all possible backgrounds to $t\bar{t}$ production in the dilepton channel is provided in section 7. Finally, a limit on the $t\bar{t}$ production cross section is calculated in section 8.

2 Lepton Selection

2.1 Trigger

For the trigger efficiencies, which are part of the acceptance calculation, we used results obtained by other people. For muons [2], the efficiencies are 95.0 $\pm$ 0.8% for Level 1, and 93.7 $\pm$ 1.4% for Level 2. For Level 3, the efficiency is 98% due to track reconstruction. The fact that muon chambers for 2 wedges have been turned off has also been taken into account. Similarly, for central electrons [3], the trigger efficiencies are 99.2 $\pm$ 0.1% for Level 1 and 94.0 $\pm$ 0.3% for Level 2 and 98.2 $\pm$ 0.1% for Level 3. For Plug electrons [4], the trigger efficiency is about 20% at E_T=20 GeV, and reaches 95% at about 35 GeV. For high P_T dilepton events, the overall trigger efficiency is about 97% (see section 6.5).

A trigger path was not explicitly required when selecting the data events, however we have checked that volunteers (i.e. not coming in with the CE, MU, or PE trigger paths) account for only $\sim$1% of the dilepton events after the P_T cuts. Furthermore, we have looked at the two events in the signal region and verified that they came in through the trigger path.

2.2 Data Sample

We use data from the L3 triggers going through the EXPRESS stream STRX_1F.
EXPRESS has inclusive electron and muon triggers with standard (tight) lepton identification cuts. The P_T (E_T) cut on the inclusive muon (electron) streams is 18 GeV. In order to be able to go lower in lepton P_T cut, we implemented a L3 dilepton filter, TDLFLT, whose output also goes to STRX_1F. The details of TDLFLT can be found in CDF$TOP_DATA:[ANA.DILEPTON]TDLFLT_DEFAULTS.TXT or directly in the code in C$TOP:TDLFLT.CDF. The filter selects events with two lepton candidates, each above a P_T threshold of 15 GeV. Lepton candidates can be central muons (CMUO's coming from CMU, CMP or CMX), minimum ionizing tracks (CMIO), central electrons, or plug electrons.

Offline, we select events with dileptons above the 15 GeV cut and tighter lepton identification cuts (see following sections) from all STRX_1F events. All data were processed with version 6.1 of the offline code.

2.3 Selection Cuts for Central Electrons

Tight cuts:

E_T	>	15 GeV (uncorrected)
P_T	>	10 GeV/c
E/P	<	2.0
HAD/EM(3 tower)	<	0.05
Δx	<	1.5 cm
Δz	<	3.0 cm
L_{shr}	<	0.2
χ^2(strip)	<	15.

Loose cuts:

E_T	>	15 GeV (uncorrected)
P_T	>	10 GeV/c
E/P	<	4.0
HAD/EM(3 tower)	<	$0.055 + 0.045E_T/100$
Δx	<	1.5 cm
Δz	<	3.0 cm
L_{shr}	<	0.2

Fiducial cuts (C$ELE:FIDELE) and a conversion removal algorithm (C$ELE:CONVERT) are applied on both loose and tight electrons.

2.4 Selection Cuts for Plug Electrons

E_T	$>$	15 GeV
HAD/EM	$<$	0.05
χ^2(3x3)	$<$	3.
VTX hit occupancy	$>$	50%
Depth χ^2	$<$	15
Iso	$<$	0.1
Track 3-D	$\geq$	3 axial superlayers

We also require that there be no additional 3-D track with $P_T > 1.5$ GeV/c within a cone of radius 0.25 around the electron track. Fiducial cuts (C$ELE:FIDELE) are also applied. Note that a calorimeter isolation cut (Iso < 0.1) is always applied on plug electrons. Here, Iso is the ratio of the total non-electron E_T in a cone of radius 0.4 around the electron, over the electron E_T.

2.5 Selection Cuts for CMUO Muons

Loose cuts:

P_T	$>$	15 GeV/c	(beam-constrained)
EM	$<$		2 GeV
HAD	$<$		6 GeV
EM+HAD	$>$		0.1 GeV
Impact parameter d0	$<$		3 mm
Z-v match	$<$		5 cm
number of axial SL	$\geq$		3
number of stereo SL	$\geq$		2
total number of SL	$\geq$		6

We also require at least one of the following: a 10 cm track match to a CMU stub, a 20 cm match to a CMP stub, or a 20 cm match to a CMX stub.

Tight cuts:

The tight cuts are identical to the loose cuts, except that the muon is required to be CMU or CMP.

2.6 Selection Cuts for CMIO Muons

P_T	$>$	15 GeV/c	(beam-constrained)
EM	$<$		2 GeV
HAD	$<$		6 GeV
EM+HAD	$>$		0.1 GeV
d0	$<$		3 mm
Z-v match	$<$		5 cm
Iso	$<$		5 GeV
number of axial SL	$\geq$		3
number of stereo SL	$\geq$		2
total number of SL	$\geq$		6

The same fiducial cuts as defined for electrons are applied on CMIO's to avoid cracks between calorimeter modules. A calorimeter isolation cut (Iso $<$ 5 GeV) is always applied on CMIO's. Here, Iso is the total energy in a cone of radius 0.4 around the muon candidate, minus the energy in the muon tower.

3 Dilepton selection Cuts

3.1 Dilepton categories

Events must contain one of the following dilepton combinations:

CE-CE	Tight central electron	-	Loose central electron
CE-PE	Tight central electron	-	Plug electron
MU-MU	Tight central muon	-	Loose central muon
MU-MI	Tight central muon	-	Minimum ionizing track (CMIO)
CE-MU	Tight central electron	-	Loose central muon
MU-CE	Tight central muon	-	Loose central electron
CE-MI	Tight central electron	-	Minimum ionizing track (CMIO)
PE-MU	Plug electron	-	Loose central muon
PE-MI	Plug electron	-	Minimum ionizing track (CMIO)

In addition, dimuon events which are back-to-back within 1.5° in azimuth and 0.1 in pseudo-rapidity are rejected on the grounds that they could be cosmic rays.

Dilepton events consisting of two CMIO's are not directly triggered on and hence are not used. A very small fraction of the total dilepton acceptance comes from events with two plug electrons; this event category has also not been included in the analysis.

The Tight central muon - Loose central electron class is temporarily removed for the Run 1A analysis. It *will* be included in Run 1B.

3.2 P_T cut

Although at the dataset level we preselect events with dilepton P_T above a 15 GeV threshold, a higher threshold is needed to minimize backgrounds from $Z \rightarrow \tau\tau$, $b\bar{b}$ and particle misidentification.

A final cut of $P_T > 20$ GeV/c is applied on both leptons. For a top mass of 120 GeV, increasing the P_T cut from 15 to 20 GeV reduces the signal by about 20%.

3.3 Invariant Mass cut

Of the Drell-Yan backgrounds, the most serious one is dielectrons and dimuons from Z^0 decay. Events are rejected if they have dielectrons or dimuons with invariant mass between 75 and 105 GeV/c^2. For $M_{top} = 160$ GeV/c^2, the efficiency of this cut on ee and $\mu\mu$ events is 80%.

3.4 Isolation cuts

For this analysis, at least one lepton is required to be central (CE, MU or MI), and to pass the track isolation cut $\sum P_T < 3$ GeV/c, where $\sum P_T$ is the sum of all the track transverse momenta in an (η, ϕ) cone of radius 0.25, excluding the lepton track. In addition, plug electrons must always pass the calorimeter and track isolation cuts described in section 2.4, and minimum ionizing tracks the calorimeter isolation cuts described in section 2.6. Figure 2 shows the track isolation $\sum P_T$ for central electrons coming from b, c, τ and W in Monte Carlo $t\bar{t}$ events, and from $Z^0 \rightarrow$ ee decays in the data.

The overall isolation cut is about 95% efficient for the $t\bar{t}$ signature (see section 6.3).

3.5 Two-jet cut for higher mass top search

For a top mass around 150 GeV/c^2, the backgrounds from WW and WZ^0 are comparable with the $t\bar{t}$ signal. The $Z^0 \rightarrow \tau\tau$ and WW, WZ^0 backgrounds in the dilepton channel can be reduced by a factor of about 6 by requiring two jets. The two-jet cut efficiency depends on the observed jet E_T and on the top mass, as shown in table 1. The efficiencies in this table are averages of Isajet with and without gluon radiation. It was verified that for a top mass of 140 GeV/c^2, the Isajet average agrees with the default Herwig calculation. The uncertainties shown are statistical only.

In the signal region we require that the jets have uncorrected $E_T > 10$ GeV and $|\eta_{det}| < 2.4$.

Efficiency of two-jet cut for top				
M_{top} (GeV/c^2)	100	120	140	160
E_T(jets) > (10,10) GeV	33.0 ± 1.4%	63.0 ± 1.3%	75.1 ± 1.0%	83.9 ± 0.9%
E_T(jets) > (15,15) GeV	22.2 ± 1.3%	45.9 ± 1.4%	62.3 ± 1.2%	74.5 ± 1.0%
E_T(jets) > (20,10) GeV	26.2 ± 1.4%	54.9 ± 1.3%	72.0 ± 1.1%	82.4 ± 0.9%

Table 1: The efficiency of the two-jet cut increases as the top mass increases

3.6 Missing E_T cut

Remaining dielectrons and dimuons from continuum Drell-Yan production are rejected by requiring significant missing E_T, namely $\not\!\!E_T > 25$ GeV. We have determined this cut by studying the $\not\!\!E_T$ distribution for Z^0 events, our aim being to minimize the Drell-Yan

background. The $\not\!\!E_T$ cut is also applied to reject dielectrons from $b\bar{b}$, fakes, and $Z^0 \to \tau\tau$ backgrounds.

It is important to note that we cut on *corrected* $\not\!\!E_T$. This corrected $\not\!\!E_T$ is calculated according to the following equation:

$$\vec{\not\!\!E}_T = \vec{\not\!\!E}_{T,\text{uncorrected}} + \sum_{\text{jets}}(\vec{E}^{\text{jet}}_{T,\text{uncorrected}} - \vec{E}^{\text{jet}}_{T,\text{corrected}}) + \sum_{\text{muons}}(\vec{E}_T^{\text{muon-tower}} - \vec{p}_T^{\,\mu}) \qquad (1)$$

where $\vec{\not\!\!E}_{T,\text{uncorrected}}$ is the raw missing transverse energy stored in the METS bank. The first sum on the right-hand side is over jets reconstructed with a cone of radius 0.4, whose uncorrected transverse energy exceeds 10 GeV and whose detector pseudo-rapidity is contained between -2.4 and $+2.4$. The corrected jet energies are obtained from routine JTC90S with option NN, that is, without subtracting the underlying event energy nor compensating for energy lost outside the jet cone. For e-μ and μ-μ events, the missing transverse energy is also corrected for the one or two high p_T muons which caused the event to be tagged as "dilepton". This is indicated by the second sum in equation (1). The vector $\vec{E}_T^{\text{muon-tower}}$ is the transverse energy measured in the calorimeter tower crossed by the muon, whereas $\vec{p}_T^{\,\mu}$ is the beam-constrained transverse momentum of the muon track in the CTC.

In the 1988-89 analysis (and in earlier versions of this analysis) we cut out dileptons with azimuthal separation $\Delta\phi_{\ell\ell} > 160°$ in order to suppress backgrounds with a back-to-back topology, such as $Z^0 \to \tau\tau$ and fake leptons. In these background events, the direction of $\vec{\not\!\!E}_T$ tends to be along the direction of a lepton or a jet. Following a suggestion by Alvin and the other Godparents, we now *remove* events with:

$$\not\!\!E_T < 50 \text{ GeV} \quad \text{AND} \quad \left(\Delta\phi(\vec{\not\!\!E}_T, \text{lepton}) < 20° \quad \text{OR} \quad \Delta\phi(\vec{\not\!\!E}_T, \text{jet}) < 20°\right) \qquad (2)$$

The above $\Delta\phi$ cuts are applied to the lepton or jet that makes the smallest angle with respect to the direction of the corrected missing E_T. The azimuthal separation between the corrected missing E_T and the nearest lepton or jet is shown in figure 1 for the $t\bar{t}$ signal. This new variable has replaced the dilepton azimuthal opening angle variable, $\Delta\phi_{\ell\ell}$, which is no longer used in our analysis. In addition to improving background rejection, the modified cuts resulted in an 8% increase of the overall efficiency.

For $M_{top} = 160$ GeV/c^2, the efficiency of the new missing E_T cuts is 69%. See section 7.4 for more discussion of these cuts.

3.7 Same-Sign Dilepton cut

The dilepton signal of $t\bar{t}$ production includes $\ell^+\ell^-$ from W^+W^-, W^+b, $W^-\bar{b}$, $b\bar{b}$, $W^+\tau^-$, $W^-\tau^+$, and $\tau^+\,\tau^-$ (where by b we mean both b and c quarks). The contribution of each channel, according to ISAJET, is listed in table 2. Numbers under the headings "GENP" were obtained at the GENP level with a P_T cut of 20 GeV/c on both leptons.

Columns labeled "QFL" were obtained after QFL detector simulation by applying the lepton identification, fiducial, transverse momentum and isolation cuts. At the GENP level, 68% of the dileptons come from W^+W^- for a top mass of 120 GeV/c^2, but only 47% for a top mass of 160 GeV/c^2.

After the QFL simulation, same sign dileptons account for only 3-6% of the top signal. By removing this small portion of our signal, we are able to reduce the fake background by almost 50% and the $b\bar{b}$ background by 30%.

M_{top} (GeV/c^2)	120 GENP	120 QFL	160 GENP	160 QFL
W^+W^-	68.1 ± 1.6	81.9 ± 1.4	46.7 ± 1.4	75.9 ± 1.5
$Wb + b\bar{b} + \tau b$ (OS)	13.9 ± 1.2	4.2 ± 0.8	23.9 ± 1.2	6.5 ± 0.9
$Wb + b\bar{b} + \tau b$ (SS)	9.8 ± 1.0	3.4 ± 0.7	22.3 ± 1.1	5.7 ± 0.8
$\tau^+\tau^- + W\tau$	7.9 ± 0.9	10.4 ± 1.1	6.7 ± 0.7	11.7 ± 1.1

Table 2: Percentages of $t\bar{t}$ dileptons according to their origin.

4 Data

After the lepton identification and P_T cuts, there are 6 eμ, 685 ee, and 571 $\mu\mu$ events.

4.1 eμ

Figure 3 shows distributions for the six events. Of the six eμ events, one has been removed because it belongs to the tight μ - loose e category. This is the so-called Pseudo-E Mu event; it satisfies all the other event topology requirements. Only two out of the remaining five events survive all the topology cuts and are in the signal region. The two signal events and the Pseudo-E Mu event are described in detail in the next section.

4.2 ee and $\mu\mu$

Figure 4a and c show the invariant mass distributions for dielectrons and dimuons, respectively. A total of 58 dielectron events and 62 dimuon events survive the Z^0 mass rejection cut. They are plotted in the $\Delta\phi(\not\!\!E_T$, lepton or jet)-$\not\!\!E_T$ plane in Figures 4b and d, respectively. After the topology cuts, no dielectron events and no dimuon events remain in the signal region.

	Run 41540 Charge	Event 127085 P_T (GeV/c)	η	ϕ (deg)
Central electron	−	22.2	0.84	32
Central muon	+	47.7	0.17	14
Central muon	+	8.8	0.18	352
Jet 1 (b-tag JETVTX)		127.5	0.11	352
Jet 1 (raw)		107.9		
Jet 2 (b-tag JETPROB)		53.0	−0.54	215
Jet 2 (raw)		44.3		
Jet 3		20.2	−2.94	112
Jet 3 (raw)		18.0		
MET(Corrected)		136.4		179
$\Delta\phi$ ($\not\!\!E_T$,lepton)				147
$\Delta\phi$ ($\not\!\!E_T$,jet)				36

Table 3: Characteristics of the DPF event. Corrected calorimeter E_T is used in the P_T column for the electron and jet clusters.

5 Comments on the candidates

5.1 Comments on the eμ candidates

5.1.1 the DPF event

The event (R41540/E127085) contains an electron with E_T = 22.2 GeV and a muon(CMP) with P_T = 47.7 GeV/c and $\not\!\!E_T$ = 136 GeV. The azimuthal angle separation between the two highest energy leptons is 18 degrees. There are three jets with large E_T (with raw E_T's of 108, 44 and 18 GeV). This event is called the DPF event. Much of the information on this top candidate is summarized in table 3.

Tony Liss has studied the CMP candidate. The muon candidate went through part of CEM and 3 absorption lengths of iron in the CMP wall. The slope matching is poor, but muons from W have long tails in the distribution. The slope matching is not used in muon analyses because it is not efficient.

From Hans Wenzel : concerning the SVX, the muon is as nice as it possibly can be. The charge and the length of the clusters are in total agreement with what you expect from a minimum ionizing particle.

There were discussions about which primary vertex one should use: the one calculated by VXGTPR or from the average beam position. From VXGTPR: x = 0.0319 $\pm$ 0.0014 cm, y = -0.0120 $\pm$ 0.0007 cm, z = -4.6538 $\pm$ 0.15 cm. From the average beam position:

	Run 45047	Event 104393		
	Charge	P_T (GeV/c)	η	ϕ (deg)
Central electron	+	24.3	0.42	255
Central muon	−	40.7	−0.36	117
Jet 1 (b-tag)		62.5	−1.20	118
Jet 1 (raw)		44.0		
Jet 2 (b-tag)		28.7	−0.95	118
Jet 2 (raw)		22.5		
MET(Corrected)		117.2		312
$\Delta\phi$ ($\not\!\!E_T$,lepton)				57
$\Delta\phi$ ($\not\!\!E_T$,jet)				165

Table 4: Characteristics of the pseudo-E Mu event. Corrected calorimeter E_T is used in the P_T column for the electron and jet clusters.

x = 0.0302 cm, y = -0.0051 cm, for z = -4.6538 cm. A fit of the beamspot gives a sigma of 37 microns. We see there is a discrepancy of about 70 microns (2 sigma) in y between the two values. The high P_T muon has basically 0 impact parameter with respect to the primary vertex as calculated by VXGTPR. If we now assume that the muon is prompt, then this favors the use of the vertex as calculated by VXGTPR.

From WeiMing Yao : conclusion for the e-μ event is that there is one solid significant track in each of the 2 jets, and possibly more in Jet 1. Further study of SVX pattern recognition in dense jets is required.

Several people, including K. Kondo, S.B. Kim, B. Harral, M. Contreras and C. Campagnari, have studied the kinematics of the event. There is a consensus that, if this event were top, the mass could marginally be consistent with being around 150 GeV. The E_T of the two jets and the missing E_T are all on the high end of the distributions.

5.1.2 the Pseudo-E Mu event

See table 4. This event is no longer included in our final sample because the tight μ - loose e category has been removed temporarily (see report regarding this event from the Godparents). The increase due to the fake lepton background would be 0.01 event for 21.4 pb^{-1}, if this event (and the tight μ - loose e category) were included in the analysis. The electron candidate with 24 GeV E_T is counted BOTH as a soft lepton AND as a jet in the Soft Lepton Tag analysis,[5] which thus classifies this event as a muon + soft electron tag + 3 jets for $t\bar{t}$ candidate. Each of the (other) two jets has a SVX tag. This event is counted as muon + 3 jets in the SVX Tag analysis[6] (with two SVX tags).

	Run 47122 Charge	Event 38382 P_T (GeV/c)	η	ϕ (deg)
Central electron	+	50.6	0.93	25
Central muon	−	37.3	−0.74	4
Jet 1		78.3	0.64	218
Jet 1 (raw)		67.0		
Jet 2		15.6	−3.31	344
Jet 2 (raw)		13.6		
Jet 3		14.4	1.34	344
Jet 3 (raw)		10.7		
MET(Corrected)		59.6		149
$\Delta\phi$ ($\not\!\!E_T$,lepton)				124
$\Delta\phi$ ($\not\!\!E_T$,jet)				68

Table 5: Characteristics of the CE MX event. Corrected calorimeter E_T is used in the P_T column for the electron and jet clusters.

5.1.3 the CE MX event

The event(R47122/E38382) contains a positron (CE) with $E_T = 50.6$ GeV and a negative muon(MX) with $P_T = 37.3$ GeV/c and $\not\!\!E_T = 59.6$ GeV. The azimuthal angle separation between the leptons is 21 degrees. There are 3 jets, with raw E_T's of 67, 14, and 11 GeV. This event is sometimes called the CEMX event. See table 5.

6 Total detection efficiency

The observed cross section is related to the $t\bar{t}$ production cross section:

$$\sigma_{obs} = \sigma_{t\bar{t}} \, B \, \epsilon_{total} \tag{3}$$

where $B = \frac{4}{81}$ is the semileptonic branching fraction into ee, $\mu\mu$, or eμ.

The total efficiency is decomposed into several parts and written as:

$$\epsilon_{total} = \epsilon_{geom \cdot p_T} \, \epsilon_{ID} \, \epsilon_{Isol} \, \epsilon_{event} \, \epsilon_{two-jet} \, \epsilon_{trigger} \tag{4}$$

The arrangement of the factors on the right-hand side of equation (4) is meant to define an order in our set of selection cuts. According to this order, the efficiency of a given cut is determined relative to a sample on which all the preceding cuts have already been applied. In particular, the isolation efficiency ϵ_{Isol} comes *after* the lepton identification efficiency ϵ_{ID}. This is in contrast with the 1988-89 analysis, where these two efficiencies were calculated in the reverse order. The change was mandated by the fact that our current analysis accepts dileptons with one non-isolated leg (section 3.4). In 1988-89 both legs had to be isolated.

The geometrical and kinematic acceptance, $\epsilon_{geom \cdot p_T}$, includes the branching fraction B. It is equal to the fraction of dileptons passing fiducial and p_T cuts, divided by 4/81. As done in reference [1], we use the Monte Carlo to determine $\epsilon_{geom \cdot p_T}$, the efficiency ϵ_{Isol} of the isolation cuts, and the efficiency ϵ_{event} of the topology cuts ($M_{\ell\ell}$, $\not\!\!E_T$). The efficiency of the lepton identification cuts is calculated from Monte Carlo, with small corrections to account for the differences between data and Monte Carlo. The trigger efficiencies are measured using data.

All these efficiency calculations are described in detail in the sections that follow. For $M_{top} = 140$ GeV/c^2, the total efficiency (including the two-jet cut and 20 GeV p_T cuts on the leptons) is 15% relative to the branching fraction of 4/81.

6.1 Geometrical and kinematical acceptance $\epsilon_{geom \cdot p_T}$

Leptons at the GENP level are matched to ELES clusters or CMUO, CMIO tracks. The fraction of dileptons inside the detector fiducial region is calculated. For the $\mu\mu$ categories, we require that at least one muon be in the CMU · CMP triggerable region. For plug electrons, the 3-D track requirement of section 2.4 is applied. Results used for the acceptance calculation are shown in table 6. A similar study, with consistent results, is presented in reference [7].

6.2 Lepton selection efficiency ϵ_{ID}

Leptons in $t\bar{t}$ events have widely varying isolation characteristics, depending on whether their parent particle is a W, a b, or a τ. Hence the identification efficiencies will also

$\epsilon_{geom \cdot P_T}$ $P_T > 20$ is applied to both leptons				
M_{top}	100	120	140	160
CE-CE	0.064 ± 0.003	0.085 ± 0.004	0.112 ± 0.004	0.114 ± 0.005
CE-MU	0.131 ± 0.005	0.175 ± 0.005	0.218 ± 0.006	0.279 ± 0.006
CE-MI	0.039 ± 0.003	0.042 ± 0.003	0.054 ± 0.003	0.053 ± 0.003
CE-PE	0.011 ± 0.001	0.013 ± 0.002	0.014 ± 0.002	0.013 ± 0.002
MU-MU	0.055 ± 0.003	0.066 ± 0.004	0.089 ± 0.004	0.114 ± 0.005
MU-MI	0.019 ± 0.002	0.022 ± 0.002	0.038 ± 0.003	0.037 ± 0.003
MU-PE	0.013 ± 0.002	0.012 ± 0.002	0.017 ± 0.002	0.018 ± 0.002
PE-MI	0.004 ± 0.001	0.004 ± 0.001	0.004 ± 0.001	0.003 ± 0.001
Total	0.337 ± 0.012	0.419 ± 0.011	0.547 ± 0.010	0.632 ± 0.009

Table 6: Geometric and kinematic acceptances for various top masses

vary according to parentage. We have used our Isajet+QFL Monte Carlo sample to estimate the lepton identification efficiencies in $t\bar{t}$ events. To correct for the difference between real data and Monte Carlo, we have subsequently multiplied these estimates by the DATA/QFL ratio of efficiencies for leptons from Z-decay.

In the next four subsections, we give the identification efficiencies of central electrons, plug electrons, central muons and minimum ionizing tracks, as determined from Z decays in real data. The calculation of lepton identification efficiencies in $t\bar{t}$ events is described in section 6.2.5.

6.2.1 Central electrons CE

The efficiency is determined from a data sample of $Z^0 \rightarrow ee$. The sample contains 394 events of the type tight-tight and 450 tight-loose. See table 7.

6.2.2 Plug electrons PE

The plug electron ID efficiency was measured using $Z^0 \rightarrow ee$, where one electron is in the central region and the other in the plug. Both electrons are required to be isolated. Our sample consists of 115 tight-loose Z's. See table 8. For this sample, our 3-d CTC track requirement on plug electrons was imposed. Only about 1/3 of the total CE-PE Z events pass this requirement. The track requirement is taken as a fiducial cut, and absorbed as part of the geometrical acceptance in the calculation of the top detection efficiency.

$Z^0 \rightarrow$ CE-CE 509 events				
Cut	Npass	ϵ		
(tight cut)				
HAD/EM < 0.05	484	0.972	$\pm$	0.005
E/P < 2.0	478	0.966	$\pm$	0.006
Δx < 1.5 cm	466	0.952	$\pm$	0.007
Δz < 3.0 cm	500	0.990	$\pm$	0.003
χ^2(Strip) $< 15.$	489	0.978	$\pm$	0.005
$L_{shr} < 0.2$	504	0.994	$\pm$	0.002
Total (tight)		0.873	$\pm$	0.011
(loose cut)				
HAD/EM $< 0.055 + 0.045E_T/100$	504	0.994	$\pm$	0.002
E/P < 4.0	509	1.000	$\pm$	0.000
Δx < 1.5 cm	466	0.952	$\pm$	0.007
Δz < 3.0 cm	500	0.990	$\pm$	0.003
$L_{shr} < 0.2$	504	0.994	$\pm$	0.002
Total (loose)		0.938	$\pm$	0.008

Table 7: Central electron selection efficiency

$Z^0 \rightarrow$ CE-PE 115 events					
	Cut	Npass	ϵ		
HAD/EM	< 0.05	113	0.983	$\pm$	0.012
χ^2(3x3)	$< 3.$	111	0.965	$\pm$	0.017
N(VTPC)	> 0.5	109	0.948	$\pm$	0.021
χ^2(depth)	$< 15.$	109	0.948	$\pm$	0.021
Combined		98	0.852	$\pm$	0.033

Table 8: Plug electron selection efficiency

6.2.3 Central muons MU

The efficiency is determined from $Z^0 \rightarrow \mu\mu$ data. There are 394 tight-loose events. The efficiency of the track quality requirement is measured to be above 0.99 using a sample of electron tracks from W$\rightarrow$ $e\nu$ decays. The efficiencies as shown in table 9 are obtained by:

eff(overall) = 2 Npass / (N + Npass)

eff(each cut) = (Npass + Npass_i) / (N + Npass)

where N (= 394) is the number of events inside the Z mass window with at least one tight muon, Npass (= 340) is the number of events with both leptons passing the tight cuts, and Npass_i is the number of events in which both muons pass the individual cut.

$Z^0 \rightarrow \mu\mu$ 394 events				
cut	Npass(_i)	ϵ		
EM	368	0.965	$\pm$	0.007
HAD	385	0.993	$\pm$	0.005
EM+HAD	392	0.997	$\pm$	0.002
dX	393	0.999	$\pm$	0.001
all	340	0.926	$\pm$	0.010

Table 9: Central muon selection efficiency

6.2.4 Minimum ionizing tracks MI

The track stub matching for the CMUO events is quite high (393/394), thus the identification cut efficiency for CMIO's is almost equal to that for CMUO's. The CMIO efficiency can be obtained from table 9 by removing the DX cut.

6.2.5 Lepton identification efficiency in $t\bar{t}$ events

As discussed in section 3.2, there are 3 sources of leptons in top events: W's, b's and τ's. On the other hand, from a detector point of view there are 6 classes of leptons: tight central electrons (TCE), loose central electrons (LCE), plug electrons (PE), tight central muons (TCM), loose central muons (LCM), and minimum ionizing tracks (MI). In table 10 we give the single lepton efficiency for the 3 sources and 6 classes of leptons. For each class, the identification efficiency is the weighted average given in equation 5, where f_W, f_b, and f_τ are the fractions of leptons passing the p_T and fiducial cuts and coming from W's, b's and τ's respectively, at the GENP level.

$$\epsilon_{ID}(\text{class}) = f_W\, \epsilon(\text{class}, W) + f_b\, \epsilon(\text{class}, b) + f_\tau\, \epsilon(\text{class}, \tau) \qquad (5)$$

The fractions f_W, f_b and f_τ depend slightly on the top mass and on the rapidity of

Single lepton ID cut efficiency M_{top} = 140 GeV/c^2				
	ϵ_W	ϵ_b	ϵ_τ	ϵ_{ID}(class)
TCE	0.794 ± 0.009	0.114 ± 0.016	0.822 ± 0.036	0.670 ± 0.014
LCE	0.872 ± 0.006	0.156 ± 0.017	0.854 ± 0.028	0.739 ± 0.014
PE	0.627 ± 0.022	0.092 ± 0.051	0.454 ± 0.122	0.520 ± 0.022
TCM + LCM	0.924 ± 0.003	0.213 ± 0.020	0.885 ± 0.020	0.775 ± 0.015
MI	0.893 ± 0.010	0.131 ± 0.043	0.829 ± 0.064	0.732 ± 0.018

Table 10: Lepton selection efficiency

the leptons considered. For M_{top} = 140 GeV/c^2 and for central electrons, the fractions are f_W=0.767±0.013, f_b=0.185±0.012, and f_τ=0.049±0.007. Similarly, the fractions for the muons are f_W=0.746±0.013, f_b=0.207±0.012, and f_τ=0.048±0.007. The efficiencies ϵ(class,W), ϵ(class,b) and ϵ(class,τ) include a small correction factor which accounts for the difference between real data and Monte Carlo. The correction ensures that the efficiencies for leptons from Z-decay measured in the data agree with those of QFL simulated Z-decay leptons. We find the DATA/QFL ratios to be 1.04, 0.99, 1.08, and 0.95 for the TCE, LCE, PE, and TCM/LCM/MI lepton classes respectively. In addition, central electron efficiencies have been degraded by 4% to account for losses due to the conversion cuts.

The total dilepton ID efficiency is obtained by summing over the eight dilepton categories. It is given in table 11. The entries in table 11 are products of the single lepton efficiencies of table 10, except for the CE-CE case where the formula $\epsilon = \epsilon_{tight}\ (2\ \epsilon_{loose} - \epsilon_{tight})$ was used to take into account correlations between tight and loose central electron cuts. In table 10, the MI efficiency is low by two sigma (4%) compared with the TCM + LCM, although these efficiencies are expected to be equal. We believe this could be a statistical fluctuation, with negligible effect in the overall detection efficiency.

6.3 Isolation cut efficiencies ϵ_{Isol}

The dilepton isolation efficiencies shown in table 12, are the fractions of dilepton events passing the P_T and lepton ID cuts, which also pass the isolation cuts. The isolation cut is very efficient because we require only one central isolated lepton in the tracking chamber for the CE-CE, CE-MU, MU-MU categories, which account for 82% of the acceptance for M_{top} = 140 GeV/c^2. In addition to requiring at least one CE, MU or MI isolated in the tracking chamber, for the CE-MI, CE-PE, MU-MI, MU-PE, and PE-MI categories (18% of the acceptance), the PE or MI leg is required to be isolated in the calorimeter, resulting in a lower isolation efficiency for these categories.

	ϵ_{ID}				
M_{top}	100	120	140	160	180
CE-CE	0.697 ± 0.017	0.636 ± 0.019	0.541 ± 0.014	0.494 ± 0.013	0.437 ± 0.011
CE-MU	0.657 ± 0.017	0.612 ± 0.019	0.519 ± 0.015	0.463 ± 0.013	0.403 ± 0.011
CE-MI	0.631 ± 0.018	0.596 ± 0.022	0.490 ± 0.016	0.451 ± 0.014	0.393 ± 0.012
CE-PE	0.451 ± 0.020	0.438 ± 0.027	0.341 ± 0.016	0.333 ± 0.016	0.294 ± 0.014
MU-MU	0.782 ± 0.018	0.724 ± 0.019	0.601 ± 0.016	0.550 ± 0.014	0.499 ± 0.013
MU-MI	0.751 ± 0.020	0.705 ± 0.023	0.568 ± 0.018	0.536 ± 0.016	0.488 ± 0.014
MU-PE	0.537 ± 0.023	0.518 ± 0.031	0.394 ± 0.019	0.396 ± 0.019	0.365 ± 0.016
PE-MI	0.516 ± 0.023	0.505 ± 0.032	0.372 ± 0.019	0.386 ± 0.019	0.357 ± 0.017
Total	0.675	0.629	0.528	0.482	0.428

Table 11: The lepton ID efficiency as a function of top mass.

	ϵ_{Isol}			
M_{top}	100	120	140	160
CE-CE	0.989 ± 0.008	0.973 ± 0.011	0.984 ± 0.008	0.988 ± 0.007
CE-MU	0.989 ± 0.005	0.986 ± 0.005	0.980 ± 0.006	0.975 ± 0.006
CE-MI	0.812 ± 0.036	0.830 ± 0.032	0.839 ± 0.030	0.782 ± 0.033
CE-PE	0.889 ± 0.105	1.000 ± 0.000	0.867 ± 0.088	0.842 ± 0.084
MU-MU	0.979 ± 0.009	0.982 ± 0.008	0.980 ± 0.008	0.988 ± 0.006
MU-MI	0.880 ± 0.036	0.856 ± 0.037	0.875 ± 0.029	0.831 ± 0.035
MU-PE	0.955 ± 0.044	0.824 ± 0.092	0.704 ± 0.088	0.926 ± 0.050
PE-MI	0.875 ± 0.117	1.000 ± 0.000	0.875 ± 0.117	1.000 ± 0.000
Total	0.959 ± 0.006	0.955 ± 0.006	0.954 ± 0.006	0.947 ± 0.006

Table 12: The isolation efficiency is approximately 95% for a top mass between 100 GeV/c^2 and 160 GeV/c^2

6.4 Event cuts efficiencies ϵ_{event}

The efficiency ϵ_{event} is the fraction of dilepton events passing the p_T and isolation cuts which also pass the following cuts combined: opposite-sign, invariant mass, and missing E_T (both in magnitude and direction). See table 13. For $M_{top} = 160$ GeV/c^2, the efficiencies of the opposite-sign and missing E_T cuts are 94% and 76%, respectively. The invariant mass cut applied in the ee and $\mu\mu$ channels is 80% efficient. The combined efficiency of the three cuts on dileptons is $\epsilon_{\text{event}} = 69\%$.

Lepton charge, $\not\!\!E_T$, $\Delta\phi(\not\!\!E_T$, lepton or jet) and $M_{\ell\ell}$ cuts.				
M_{top}	100	120	140	160
CE-CE	0.52 ± 0.04	0.55 ± 0.03	0.59 ± 0.03	0.57 ± 0.03
CE-MU	0.73 ± 0.02	0.71 ± 0.02	0.75 ± 0.02	0.75 ± 0.02
CE-MI	0.71 ± 0.05	0.67 ± 0.04	0.78 ± 0.03	0.71 ± 0.04
CE-PE	0.50 ± 0.18	0.59 ± 0.12	0.67 ± 0.13	0.50 ± 0.13
MU-MU	0.61 ± 0.03	0.61 ± 0.03	0.54 ± 0.03	0.58 ± 0.03
MU-MI	0.60 ± 0.06	0.58 ± 0.06	0.50 ± 0.05	0.55 ± 0.05
MU-PE	0.71 ± 0.10	0.64 ± 0.13	0.87 ± 0.07	0.76 ± 0.09
PE-MI	0.71 ± 0.17	0.86 ± 0.13	0.91 ± 0.13	1.0 ± 0.00
Total	0.659 ± 0.014	0.662 ± 0.013	0.694 ± 0.012	0.688 ± 0.012

Table 13: Event topology cut efficiencies for several top masses

6.5 Trigger efficiencies

The single lepton (central electron, plug electron, CMU*CMP muon) triggers of section 2.1 are convoluted with the lepton spectra of dileptons passing the geometry, P_T, and isolation cuts. For dilepton events in categories that can be collected with two of the lepton triggers, the trigger efficiency is computed as $1-f_1f_2$, where f_1 and f_2 are the separate probabilities of failing the first and second lepton triggers, respectively. A summary of dilepton trigger efficiencies is shown in table 14.

6.6 Total detection efficiencies ϵ_{total}, and systematic uncertainties

Table 15 shows the detection efficiency as a function of top mass for each dilepton category. The sums over dilepton categories are also provided. Efficiency plots for a) the

	$\epsilon_{\text{trigger}}$			
M_{top}	100	120	140	160
CE-CE	0.993	0.993	0.993	0.993
CE-MU	0.989	0.989	0.989	0.989
CE-MI	0.916	0.916	0.916	0.916
CE-PE	0.983	0.983	0.979	0.983
MU-MU	0.983	0.983	0.983	0.983
MU-MI	0.869	0.869	0.869	0.869
MU-PE	0.973	0.974	0.967	0.973
PE-MI	0.797	0.803	0.745	0.797
Total	0.972	0.974	0.972	0.976

Table 14: Trigger efficiency

	ϵ_{total}				
M_{top}	100	120	140	160	180
CE-CE	0.007	0.018	0.026	0.026	0.032
CE-MU	0.020	0.047	0.062	0.078	0.080
CE-MI	0.004	0.008	0.012	0.010	0.011
CE-PE	0.001	0.002	0.002	0.002	0.002
MU-MU	0.008	0.018	0.021	0.029	0.032
MU-MI	0.002	0.004	0.006	0.007	0.010
MU-PE	0.002	0.002	0.003	0.004	0.005
PE-MI	0.000	0.001	0.001	0.001	0.001
Total	0.045	0.100	0.134	0.157	0.173

Table 15: Total efficiency

	$\epsilon_{\text{geom}\cdot P_T}$	ϵ_{ID}	ϵ_{Isol}	ϵ_{event}	$\epsilon_{\text{two-jet}}$	$\epsilon_{\text{Trigger}}$	ϵ_{total}
CE-CE	11.2	54.1	98.8	59.1	75.1	99.3	2.6
CE-MU	21.8	51.9	98.3	75.1	75.1	98.9	6.2
CE-MI	5.4	49.0	84.6	78.3	75.1	91.6	1.2
CE-PE	1.4	34.1	85.7	66.7	75.1	97.9	0.2
MU-MU	8.9	60.1	98.4	54.0	75.1	98.3	2.1
MU-MI	3.8	56.8	87.7	50.2	75.1	86.9	0.6
MU-PE	1.7	39.4	79.5	87.1	75.1	96.7	0.3
PE-MI	0.4	37.2	91.7	90.9	75.1	74.5	0.1
Total (%)	54.7	52.8	95.4	69.4	75.1	97.3	13.4

Table 16: Dilepton efficiency for a top mass of 140 GeV/c^2

new '92 standard cuts, and b) after the additional two-jet cut, are shown in Figures 5a and 5b respectively. In table 16 a rundown is given of all the individual efficiencies which contribute to the total detection efficiency for a top mass of 140 GeV/c^2.

The systematic uncertainty on the detection efficiency comes mainly from the modeling of gluon radiation, the detector simulation, the jet energy scale, and limited Monte Carlo statistics. We have separately investigated the systematic uncertainty for each component of the detection efficiency. This is discussed below, for the case where the two-jet cut is *not* applied:

1. Geometrical and kinematical acceptance. Here, one source of systematic uncertainty is the modeling of initial state radiation. Initial state radiation affects the motion of the $t\bar{t}$ system and hence the rapidity and transverse momentum distributions of the top quark decay products. This effect can be studied by turning on and off gluon radiation in Isajet. Another systematic uncertainty results from the choice of structure functions. This work is still in progress. Our preliminary estimate is 3% for the total systematic uncertainty on the geometrical and kinematical acceptance.

2. Lepton identification. The modeling of gluon radiation affects the isolation properties of the leptons, and hence their identification efficiency. We have studied this effect by turning on and off gluon radiation in Isajet, and taking half the difference in the corresponding lepton identification efficiencies as systematic uncertainty. This gives 2.4%. Detector simulation also affects lepton identification. Here, we take half the difference between the result obtained from CDFSIM and that obtained from QFL; this is 5%. Since these two contributions are clearly independent, the systematic uncertainty on lepton identification is $2.4\% \oplus 5\% = 6\%$.

3. Lepton isolation. The technique for determining the systematic uncertainty on

lepton isolation is the same as for lepton identification. The effects of gluon radiation and detector simulation are both 1%. Hence the combined systematic uncertainty is (conservatively) $1\% \oplus 1\% = 2\%$.

4. Effect of jet energy scale on missing ET correction. Since we correct the missing ET for the jet energy scale, and subsequently cut on corrected missing ET, a small systematic uncertainty must be expected from this source. By varying the jet energy scale by $\pm 10\%$, and taking half the corresponding difference in acceptance as systematic uncertainty, we find 2%.

5. Monte Carlo statistics. This is about 3%.

The sum in quadrature of all the uncertainties listed above is 8%. These uncertainties are essentially independent of top mass. On the other hand, the systematic uncertainty on the two-jet cut efficiency varies strongly with top mass. This is shown in table 17. The two-jet cut efficiency depends on the modeling of gluon radiation and on the jet energy scale. The uncertainty due to the former was obtained from Isajet by turning gluon radiation on and off and taking half the difference in the resulting efficiencies. Similarly, by changing the jet energy scale by $\pm 10\%$ we determined the systematic uncertainty due to the latter. In addition to the uncertainties discussed so far, one has to include the

Systematic error in ϵ_{total} (%)				
M_{top}	100	120	140	160
Two-jet cut (gluon radiation)	36	12	6	3
Two-jet cut (energy scale)	5	4	2	1
All other cuts	8	8	8	8
Total	38	15	10	9

Table 17: Systematic uncertainties in $t\bar{t}$ detection efficiency

uncertainty on the luminosity measurement, which we take to be 10%.

The expected number of events as a function of top mass and dilepton category is shown in table 18. Table 19 lists the expected numbers of events without the two-jet cut, with the two-jet cut, and with the two-jet cut and including the tight μ - loose e dilepton category.

Number of event expected in 21.4 pb^{-1}					
M_{top}	100	120	140	160	180
CE-CE	0.808	0.743	0.472	0.228	0.141
CE-MU	2.188	1.923	1.109	0.674	0.358
CE-MI	0.463	0.331	0.217	0.088	0.051
CE-PE	0.077	0.088	0.036	0.013	0.011
MU-MU	0.895	0.728	0.375	0.253	0.144
MU-MI	0.238	0.173	0.111	0.057	0.045
MU-PE	0.167	0.084	0.062	0.035	0.020
PE-MI	0.037	0.033	0.013	0.008	0.003
total	4.87	4.10	2.39	1.36	0.77

Table 18: Total number of top events expected as a function of the top mass

M_{top} (GeV/c^2)	100	120	140	160	180
$\sigma_{t\bar{t}}$ (pb)	102	38.9	16.9	8.16	4.21
Without two-jet cut:					
ϵ_{total} B (%)	0.68	0.78	0.88	0.933	0.97
Events in 21.4 pb^{-1}	14.8	6.5	3.2	1.6	0.9
With two-jet cut:					
ϵ_{total} B (%)	0.22	0.49	0.66	0.78	0.86
Events in 21.4 pb^{-1}	4.9	4.1	2.4	1.4	0.8
With two-jet cut and including tight μ - loose e category:					
ϵ_{total} B (%)	0.24	0.52	0.69	0.83	0.92
Events in 21.4 pb^{-1}	5.2	4.3	2.5	1.5	0.8

Table 19: Cross sections for $t\bar{t}$ and number of events for three sets of cuts

7 Background studies

7.1 $Z^0 \rightarrow \tau\tau$

Rather than use a Monte Carlo to generate the $Z^0 \rightarrow \tau\tau$ background, we have used our data sample of 1113 $\gamma/Z^0 \rightarrow e\,e$ events. In each event we replaced the electrons with tau's of the same p_T. The tau's were then decayed into the electron or the muon channel. We have simulated 1113 $\times$ 80 such events. Figure 6 shows distributions of several reconstructed variables (these are the same variables as given for a top mass of 140 GeV/c^2 in Figure 1). The event topology cut efficiencies extracted from this simulation sample are given in table 20.

Cut:	Mass window	$\Delta\phi$ ($\not\!\!E_T$,lepton or jet)	$\not\!\!E_T$	Additional 2 jet cut
Efficiency:	0.84	0.38	0.15	0.31

Table 20: Event topology cut efficiencies for the $Z^0 \rightarrow \tau\tau$ background with a (20,20) P_T cut.

We also generated three Isajet+QFL samples, each with 30k events and a different value of the parameter QTW which governs the transverse momentum of the Z. These samples were used to get the efficiencies for the geometry, p_T, ID, and isolation cuts.

The overall yields were normalized by taking the $Z^0 \rightarrow \tau\tau$ cross section to be equal to the $Z^0 \rightarrow ee$ cross section measured at CDF [8], and a branching fraction of the τ pair into dileptons B = $(0.178 \times 2)^2 = 0.127$. The number of events we expect in 21.4 pb^{-1} is given in table 21.

For more details on the $Z^0 \rightarrow \tau\tau$ background, see reference [9].

7.2 $Z^0 \rightarrow b\bar{b}$

This background has been generated using ISAJET and simulated with QFL and reconstructed. 740 K were generated corresponding to an integrated luminosity of 841 pb^{-1}. No events were found in the signal region when the nominal cuts (no two jet cut) were applied. This gives a limit of less than 0.025 events for a run of 21.4 pb^{-1}. If the two jet cut reduces this by a factor of 3, as it does for $Z^0 \rightarrow \tau\tau$, then this background is less than 0.01 events. We therefore do not consider this background further.

	p_T cut at (15,15)	P_T cut at (20,20)
Before topology cut	16.9 ± 0.9	7.5 ± 0.4
After topology cut	1.11 ± 0.15	0.42 ± 0.08
additional 2 jets E_T > 10 GeV	0.34 ± 0.07	0.13 ± 0.03

Table 21: Number of events expected from the $Z^0 \rightarrow \tau\tau$ background for a run of 21.4 pb^{-1}

7.3 Background from WW and WZ^0

We use the ISAJET (6.43) Monte Carlo, normalized to a total WW cross section of 9.53 pb. See Ohnemus [10]; we took the result for HMRSB structure functions. Before jet cuts, ISAJET predicts 1.17 ± 0.35 dilepton events from WW (see table 22). Figure 7 shows the standard reconstructed variables for this background. Here we have assigned a 30% uncertainty due to theoretical uncertainties in the cross section. With a jet threshold of 10 GeV, 13% of these events will pass the two-jet cut. Since the ISAJET prescription for gluon radiation is esentially unconfirmed, we checked the two-jet rejection factor by examining a matrix element Monte Carlo. Michelangelo Mangano provided a calculation predicting that the efficiency of the two-jet cut should be approximately 2.7 times higher at typical WW subprocess energies of 300 GeV than at subprocess energies of 90 GeV. We can use this Monte Carlo shape for the mass variation and at 90 GeV we can use Z data (again !) for calibration. The data show that 4.1 ± 0.6 % of Z events have two jets above 10 GeV. Therefore the two-jet cut efficiency for WW can be estimated as 2.7×4.1%=11%. Since the agreement between this estimate and ISAJET is good, we simply use the ISAJET two-jet cut efficiency and assign a 30% systematic uncertainty on it.

It is worth noting that we also tried Tao Han's WW + 2jet Monte Carlo and found the efficiency of the two-jet cut to be approximately 2%. This is clearly in contradiction with the data since we know that the Z's, at lower mass, have 4%. The study was inconclusive in this regard, however it is interesting to note that several 2-jet matrix element Monte-Carlos tend to underestimate the jet activity. Mangano's Monte Carlo, for instance, predicts that 3.2% of Z's will have two jets with parton P_T > 15 GeV.

The expected contribution from WZ^0 production for 21.4 pb-1 is 0.065 before the TWO-JET cut, This background is negligible.

Lepton P_T thresh.	Jet E_T thresh.	$e\mu$	ee, $\mu\mu$	Total
20 GeV	None	0.74±0.22	0.43±0.13	1.17±0.35
20 GeV	10 GeV	0.097±0.041	0.057±0.024	0.15±0.06
20 GeV	15 GeV	0.061±0.026	0.036±0.015	0.10±0.04
15 GeV	None	0.86±0.26	0.51±0.15	1.37±0.41
15 GeV	10 GeV	0.11±0.05	0.07±0.03	0.18±0.08

Table 22: Number of WW events expected in 21.4 pb^{-1}.

7.4 Dielectron and Dimuon Backgrounds from Drell-Yan

The $t\bar{t}$ signature can also be mimicked by dilepton final states of Drell-Yan events ($\gamma/Z^0 \rightarrow ee, \mu\mu$). We use the observed $Z^0 \rightarrow ee$, and $Z^0 \rightarrow \mu\mu$ distributions to predict the background from the continuum. Rejection factors for the missing E_T and jet cuts obtained from Z events are applied to the Drell-Yan events outside the Z-window. Our initial assumption is that the $P_T(\gamma, (Z^0)$ distributions inside and near the Z^0 region are similar. ISAJET and other Monte Carlos predict that there is a slight stiffening with increasing mass in the $P_T(\gamma,Z^0)$ and jet distributions which could lead to an overestimate of the background. Therefore, a (small) Monte Carlo correction is applied to account for the mass dependence of the P_T and jet activity. We use two-jet cut efficiencies as a function of mass provided by Michelangelo Mangano from a boson+2jet matrix element Monte Carlo. We find that for our cuts, using the jet activity from Z^0 events and assigning it to events outside the Z^0 mass window requires a correction factor of 0.87.

In Figure 8 a there are 1151 dielectron and dimuon events in the Z-mass region, between 75 and 105 GeV/c^2. There are 88 events below the window, and 35 above. Figure 8 b shows the comparison of corrected and uncorrected $\not\!\!E_T$, and it is seen that the corrected quantity gives better rejection. Figures 8 c and d show the jet multiplicity distributions before and after the $\not\!\!E_T$ cut of 25 GeV.

The large $\not\!\!E_T$ in Z^0 events originates frequently from jet mismeasurement. In those cases the direction of the $\not\!\!E_T$ is along one of the jets. To obtain greater rejection against Drell-Yan we have developed the cut outlined in Fig 8 e and f, requiring that the $\not\!\!E_T$, if lower than 50 GeV, be more than 20 degrees away from the closest jet. The definition of the cut was chosen from looking at Fig 8 e for Z + 1 jet events. A similar cut requiring that the $\not\!\!E_T$, if lower than 50 GeV, be more than 20 degrees away from the closest lepton, was developed to reject $Z^0 \rightarrow \tau\tau$ events where there can be neutrinos along the lepton direction. This second cut is not needed for direct Drell-Yan dielectron and dimuon production backgrounds, but the distributions are shown for reference in Fig 8 g and h.

After the signal cuts, including the two-jet cut, there is one event in the Z-region. When scaled back, this gives a background expectation of 0.10 ± 0.10 events in the top dilepton signal region. Some results for different cuts are summarized in tables 23 and 24.

For more details see reference [11].

Fraction of events passing different $\not\!\!E_T$ cuts	
$\not\!\!E_T$ (UNcorr) > 20 GeV	2.8%
$\not\!\!E_T$ (corr) > 20 GeV	2.3%
$\not\!\!E_T$ (UNcorr) > 25 GeV	1.4%
$\not\!\!E_T$ (corr) > 25 GeV	0.8%

Table 23: Missing E_T cut efficiency for Drell-Yan events

7.5 Background from heavy flavor events ($b\bar{b}$)

Large ISALEP + CLEO $b\bar{b}$ Monte Carlo samples have been generated for studies of high P_T leptons from B decays as a background in top searches [12]. By comparing a 67.5 pb^{-1} Monte Carlo sample to the dilepton data, we determine that after all cuts, the background contribution from $b\bar{b}$ sources to high P_T dilepton top is 0.10 $\pm$ 0.05 events normalized to 21.4 pb^{-1} of run 1A data.

Two data sets have been generated, the first having an integrated luminosity of 16.3 pb^{-1}, the second having 51.2 pb^{-1}. The first sample retains inclusive single leptons from B decays. The second keeps dileptons in which the P_T of both leptons is greater than 10 GeV. The events are generated using ISAJET with the internal loop turned on to speed up heavy quark production processes. With the multi-evolving technique, ISAJET attempts to simulate the next to leading order (NLO) $b\bar{b}$ production processes such as gluon splitting and flavor excitation. We keep events that have at least one b quark with $P_T > 25$ GeV (this corresponds to keeping 90% of the events in which the daughter leptons have $P_T > 15$ GeV). Next, the event is passed through the CLEO MC Module, which

Lepton P_T thresh.	Jet E_T thresh.	ee,$\mu\mu$
20 GeV	None	0.28$\pm$0.17
20 GeV	10 GeV	0.10$\pm$0.10
20 GeV	15 GeV	0.10$\pm$0.10
15 GeV	None	0.46$\pm$0.27
15 GeV	10 GeV	0.15$\pm$0.15
15 GeV	15 GeV	0.15$\pm$0.15

Table 24: Number of Drell-Yan background events expected in 21.4 pb^{-1}.

redecays the B mesons in the event. This changes the average charged particle multiplicity and energy flow around the lepton (We think that the CLEO B decay package is a better model than ISAJET for B physics). After making the selection cuts at the GENP level(for the first sample we require that the P_T of a single lepton be greater than 10 GeV/c) and then pass them through the QFL simulation. We use two samples to analyze, one a high statistics sample with cuts on the dileptons of (15, 15), and the other with dilepton cuts of (20, 20). The (15, 15) sample allows us to determine the rejection factors for $\not\!\!E_T$ as well as the opening angle cut. The correlation between $\not\!\!E_T$ and lepton E_T was checked by varying the P_T of one of the leptons to 17, 19, and 21 GeV/c. A 30% change was observed and this contributes the major part of the uncertainty assigned to the rejection factor for $\not\!\!E_T$. No strong correlation between the lepton P_T and the lepton-$\not\!\!E_T$and jet-$\not\!\!E_T$opening angle was observed. The number of events passing the (20, 20) cuts is used to determine the normalization. Figure 9 shows the standard reconstruction variables for this background. A normalization factor of 1.04 (= 0.94 / 90%) was determined by finding 184 eμ data events (13.1 pb^{-1}) and 196 Monte Carlo events (16.3 pb^{-1}) with (15, 5) P_T selection. The number of background events expected in our data sample is given in table 25.

	P_T cut at (15,15)	P_T cut at (20,20)
P_T, Iso, Opp-Sgn Cuts	24 $\pm$5	2.8 $\pm$0.6
Additional Missing E_T Cut	1.91 $\pm$ 0.96	0.22 $\pm$ 0.12
Additional Two-Jet Cut	0.83 $\pm$ 0.43	0.10 $\pm$ 0.05

Table 25: Number of events expected from $b\bar{b}$ background for a run of 21.4 pb^{-1}.

7.6 Background from fake

Events with a lepton and jets (for example, from W +jet production) can mimic signal events in the dilepton search if one of the jet fakes a lepton. These events may also have large missing E_T, and maybe difficult to distinguish kinematically from top events. Since this is a very important study for our analysis, two independent studies have been performed and documented [13, 14]. The procedure employed for estimating the background is to a) estimate the probability of a jet to fake a lepton, b) find how many events with lepton+jet would be in the signal region if the jet faked a lepton, and c) multiply the number of events found in b) by the fake rates found in a). In one of the studies the fake rates were determined from the Jet 20 sample (the other study used both Jet 20 and Jet 50). Central and plug ELES clusters, CMUO tracks, and CMIO tracks are selected with minimal cuts. The probability to pass the standard electron and muon identification is then measured. The fake rates are determined separately for central isolated and non-isolated tracks or clusters. This separation is necessary because in the dilepton selection, all events are required to have at least one central(CE, MU or MI) isolated lepton.

When looking through the jet data for jets which fake leptons, we will also find some real leptons from b decay. The effect of this is to increase the fake probability we would get from light quark jets alone. It is desirable to use fake probabilities which have the contributions from b quarks subtracted. To accomplish this, we refer to a study [15] which estimates the b fraction of ELES banks which pass our tight central electron cuts to be 46% $\pm$ 8%. We use this number both to scale back the fake probabilities for central electrons, and also as an indicator of the number of CMUO banks we should expect from b's in the jet data. We multiply the number of central electrons we expect from b decay by the ratio of acceptances for CMUO muons and central electrons, and use this as our estimate of the number of CMUO muons we expect from b in the jet data. We do not perform the b subtraction for plug electrons or CMIO muons because we expect the calorimeter isolation cuts on these categories to reduce the b contamination. We don't apply the 2 jet cut and opposite sign cuts when counting events which have one good lepton and one lepton bank passing the relaxed cuts. Assuming the relaxed lepton track is from a hadron, we expect its sign to be uncorrelated with the sign of the good lepton. We therefore count both opposite sign and same sign events, and divide by 2 to get the expectation for opposite sign alone. There are 15 opposite sign events and 10 same sign events. The statistics suffer badly when the 2 jet cut is applied. We have looked at W+jet events to find the rejection factor of the 2 jet cut after the other topology cuts are applied, and we use this rejection factor to obtain the number of events we expect in the signal region. Tables 26 and 27 show the expected numbers of background events for 15-15 and 20-20 lepton P_T cuts, before and after the 2-jet cut is applied.

One should note that this was in very good agreement with our other study [14] on June 28, 1993. Figure 10 shows some of the standard reconstructed variables for the fake background [14]. Because these fake leptons are predominantly in W + jets events, the event topology and kinematics can mimic top dilepton events. The cuts have been modified and the b quarks subtracted since June, so that reference [14] is quantitatively out of date. Our latest results are based on reference [13].

7.7 Background Summary and Checks

The top signal and background estimates for the present run are summarized in table 29 and 28. The total background is 0.56$\pm$0.14 events after all cuts and the data yield is 2 events. When releasing the two-jet requirement, we expect 2.5$\pm$0.5 events and observe (the same) 2 events. For the Drell-Yan background in the first column of table 28, before missing E_T and jet cuts, but after mass cuts, we used the Isajet prediction for the ratio of the numbers of events inside and outside the Z-window, together with the observed number of events in the Z-window.

A better statistics check was done in the $e\mu$ channel by lowering the P_T threshold to 15 GeV and comparing the background prediction with the number of events observed in the data after isolation cuts. Our results are shown in table 30. There is good agreement

Fake Background in 21.4 pb^{-1} Before 2-jet Cut		
Category	15 GeV Lepton P_T Cuts	20 GeV Lepton P_T Cuts
CE-CE	.339±.168	.169±.111
CE-PE	<.034	<.033
MU-MU	.140+.257−.140	.073+.238−.073
MU-MI	.091±.064	.022+.038−.022
CE-MU	.385±.300	.111+.240−.111
CE-MI	.148±.102	.061±.051
PE-MU	<.023	<.023
PE-MI	<.028	<.028
TOTAL	1.10±.41	.436±.292
SS Data	1	0

Table 26: Expected background due to hadron misidentification for 15 GeV and 20 GeV lepton P_T cuts. All cuts except for the 2-jet cut are applied. Also shown are the number of same-sign events found in the data for these cuts.

Fake Background in 21.4 pb^{-1} After 2-jet Cut		
Category	15 GeV Lepton P_T Cuts	20 GeV Lepton P_T Cuts
CE-CE	.056±.028	.028±.018
CE-PE	<.006	<.005
MU-MU	.023+.042−.023	.012+.039−.012
MU-MI	.015±.010	.004+.006−.004
CE-MU	.063±.049	.018+.039−.018
CE-MI	.024±.017	.010±.008
PE-MU	<.038	<.038
PE-MI	<.005	<.005
TOTAL	.181±.068	.072±.048
SS Data	0	0

Table 27: Expected background due to hadron misidentification for 15 GeV and 20 GeV lepton P_T cuts after the 2-jet cut is applied. Also shown are the number of same-sign events found in the data for these cuts.

		Without $\not\!\!E_T$ and two-jet cuts	Without two-jet cut	All cuts
$e\mu$	WW	1.1	0.74	0.10±0.04
	$Z \rightarrow \tau\tau$	3.7	0.22	0.07±0.02
	$b\bar{b}$	1.2	0.10	0.04±0.03
	Fake	1.2	0.19	0.03±0.03
	Total background	7.2	1.25	0.24±0.06
	CDF data	5	2	2
$ee, \mu\mu$	WW	0.6	0.43	0.06±0.02
	$Z \rightarrow \tau\tau$	3.0	0.20	0.06±0.02
	$b\bar{b}$	1.6	0.12	0.05±0.03
	Fake	1.7	0.25	0.04±0.03
	Drell-Yan	113	0.28	0.10±0.10
	Total background	120	1.28	0.31±0.11
	CDF data	120	0	0

Table 28: Number of background events expected 21.4 pb^{-1} and the number of events observed in the data.

between the background prediction and the data. As an additional check of the reliability of our background predictions, in reference [13] we compared the number of same-sign events observed in the data with a P_T threshold of 15 GeV after isolation cuts, with predictions from fakes and $b\bar{b}$. We find that the sum of the $b\bar{b}$ and fake predictions is 19.8 ± 4.0, compared to 10 same-sign events observed in the data. Again the agreement is good, although there is room to believe that our backgrounds could be somewhat overestimated and therefore conservative.

Number of top events expected in 21.4 pb^{-1}	
Top 100 (20,20)	4.87
Top 120 (20,20)	4.10
Top 140 (20,20)	2.39
Top 160 (20,20)	1.36
Top 180 (20,20)	0.77

Table 29: Total number of top events expected as a function of the top mass

		$P_T > 15$ GeV/c, Isolation, and opp.-charge requirement
$e\mu$	WW	1.2±0.4
	$Z \rightarrow \tau\tau$	8.3±0.5
	$b\bar{b}$	10±2
	Fake	5.9±1.8
	Total background	25±3
	CDF data	18

Table 30: Number of $e\mu$ background events expected in 21.4 pb^{-1} and the number of opposite-charge dilepton events observed in the data after isolation cuts and a P_T threshold of 15 GeV/c.

8 The $t\bar{t}$ Production Cross Section

The $t\bar{t}$ production cross section can be written as :

$$\sigma_{t\bar{t}} = \frac{N_{top}}{\int \mathcal{L}dt \; \epsilon_{top}} \tag{6}$$

where N_{top} is the background subtracted number of observed events, $\int \mathcal{L}dt$ is the integrated luminosity of the data sample, and $\epsilon_{top} = Br \cdot \epsilon_{total}$ is the efficiency for observing top events in the selected channel. The uncertainty in ϵ_{total} was discussed at length in section 6.6, and summarized in table 17.

Figure 12 shows our 1992-93 measurement of $\sigma_{t\bar{t}}$ as a function of M_{top}. This measurement uses equation (6) and is based on our analysis *with* the two-jet cut. We observed 2 events in a sample of 21.4 pb^{-1} and expect a background of 0.56 ± 0.14 events. The uncertainties are the sum in quadrature of the statistical uncertainty on the number of observed events, the systematic uncertainty on the acceptance (a function of top mass), and the uncertainty on the luminosity (10%). The cross section measurement is summarized in table 31.

M_{top} (GeV/c^2)	120	140	160	180
$\epsilon_{total} \cdot B$ (%)	0.49	0.66	0.78	0.86
$\sigma_{t\bar{t}}$ (pb)	13.73	10.20	8.627	7.824

Table 31: Total detection efficiency and measured cross section for $t\bar{t}$ production, as a function of top mass. These numbers are based on 21.4 pb^{-1} of data, two events in the signal region, and an expected total of 0.56 ± 0.14 background events.

This measurement can be compared with a QCD calculation to order α_s^3 of the heavy quark production cross section by Nason et al. (ref. [17, 18, 19]). The result of this work is shown as two parallel solid lines crossing figure 12 diagonally. The upper solid line represents the central value of the calculation, whereas the lower solid line is an estimated lower limit. Also shown is the result of a somewhat improved calculation by Laenen et al. (ref. [20]). The central value and lower limit on this computation are given as dot-dashed lines. The intersection of our cross section measurement with the Nason et al. central value is $M_{top} = 155$ GeV/c^2, $\sigma_{t\bar{t}} = 8.9$ pb. The intersection with the Laenen central value is $M_{top} = 158$ GeV/c^2, $\sigma_{t\bar{t}} = 8.7$ pb.

We have used our analysis *without* the two-jet cut to calculate 95% confidence level upper limits on the $t\bar{t}$ cross section. There are several ways of doing this: with and without background subtraction, with and without adding the 1988-89 data. All four combinations are drawn in fig. 12. The method we used to subtract the background and take uncertainties into account is explained in appendix A. When using the 1992-93

data alone, the number of events observed is 2 in a sample of 21.4 pb^{-1}, the expected background is 2.5 ± 0.5 events, the uncertainty on the acceptance is 8% and that on the luminosity is 10%. By adding in the 1988-89 data, the integrated luminosity becomes 25.5 pb^{-1}, the number of events observed remains 2, and the expected background becomes $(2.5 \pm 0.5) + (0.5 \pm 0.3) = (3.0 \pm 0.6)$ events. To calculate upper limits with the combined 1988-89 and 1992-93 data sets, we used the following formula:

$$\sigma_{t\bar{t}}^{\text{upper limit}} = \frac{N^{\text{upper limit}}}{(\int \mathcal{L}_{89}\, dt\ \epsilon'_{89} + \int \mathcal{L}_{93}\, dt\ \epsilon_{93}) \cdot \text{Br}} \tag{7}$$

where ϵ_{93} is the acceptance of the 'new' analysis with the 'new' detector, whereas ϵ'_{89} is the acceptance of the 'new' analysis with the 'old' detector. We believe that ϵ'_{89} is somewhat larger than ϵ_{93}, because of the reduced 1993 muon trigger acceptance (the 1993 muon trigger requires a CMU-CMP coincidence in the ϕ regions where CMP covers CMU). This only affects dimuon events (electron-muon events come in with the electron leg), so that the difference between the two acceptances should not be more than a few %. We made the conservative choice of setting $\epsilon'_{89} = \epsilon_{93}$; this slightly increases the upper limits on the cross section. For each of these upper limits, we have calculated 95% confidence level lower limits on the top mass as the intersection of the experimental upper limit with the two theoretical lower limits (Ellis and Laenen). This is summarized in table 32.

	1992-93 only		1988-89 and 1992-93 combined	
	Straight	Background subtracted	Straight	Background subtracted
Ellis	111	119	115	125
Laenen	116	124	121	130

Table 32: 95% confidence level top mass limits in GeV/c^2

A Calculation of Upper Limits on Poisson Processes

In this appendix we briefly present and justify the equations we used to calculate upper limits on the $t\bar{t}$ production cross section. Our method is a slight extension of the procedure described in detail in reference [21] and summarized in the Review of Particle Properties by the Particle Data Group. In section A.1 we describe the calculation of upper limits in the simplest case, namely when there are no backgrounds and no systematic uncertainties. Next we consider the case where there is background, and in the final section we incorporate the effect of systematic uncertainties.

A.1 Upper Limits without Background or Systematic Uncertainties

Suppose we measure the rate of some process, and observe n_0 events. The 95% confidence level upper limit N on the Poisson parameter μ_S for this process is defined to be that value of μ_S for which it would be exactly 95% probable that a random measurement of the rate would yield n_0 events or more. Hence this upper limit N is the solution of:

$$\mathrm{CL} = \sum_{n=n_0+1}^{\infty} \frac{e^{-N} N^n}{n!} \tag{8}$$

where CL is the desired confidence level. Equivalently:

$$1 - \mathrm{CL} = \sum_{n=0}^{n_0} \frac{e^{-N} N^n}{n!} \tag{9}$$

A.2 Upper Limits with Background

When backgrounds are present, the definition of upper limit must be modified to incorporate our knowledge of the fact that the actual number of events resulting from background, n_B, must be smaller than or equal to the observed number of events n_0. Let μ_B be the expectation value for the sum of all backgrounds. The probability for observing n_B background events, given the constraint $n_B \leq n_0$, is simply the Poisson probability renormalized to the allowed range of n_B:

$$P'(n_B; \mu_B) = \frac{e^{-\mu_B} \mu_B^{n_B}}{n_B!} \Bigg/ \sum_{n=0}^{n_0} \frac{e^{-\mu_B} \mu_B^{n}}{n!} \tag{10}$$

On the other hand, the probability for observing n_S signal events is still:

$$P(n_S; \mu_S) = \frac{e^{-\mu_S} \mu_S^{n_S}}{n_S!} \tag{11}$$

Hence the probability for observing a total of $n = n_B + n_S$ events, with the constraint $n_B \leq n_0$, is given by:

$$P^{\star}(n;\mu_B,\mu_S) = \sum_{n_B=0}^{\min(n,n_0)} P'(n_B;\mu_B)\, P(n-n_B;\mu_S) \tag{12}$$

Note that, because of the normalization (10), $P^{\star}(n;\mu_B,\mu_S)$ is different from the joint probability for observing $n_B \leq n_0$ background events and $n - n_B$ signal events. On the other hand, this normalization ensures that the following relation is satisfied:

$$\sum_{n=0}^{\infty} P^{\star}(n;\mu_B,\mu_S) \;=\; 1.0 \tag{13}$$

The 95% confidence level upper limit N on μ_S is now defined as that value of μ_S for which it would be 95% probable that a random repeat of the same experiment would yield a total of at least n_0 events, given that the number of background events is restricted to be less than or equal to n_0. This upper limit N satisfies the equation:

$$1 - \mathrm{CL} \;=\; \sum_{n=0}^{n_0} P^{\star}(n;\mu_B,N) \tag{14}$$

$$\;=\; \sum_{n=0}^{n_0} \frac{e^{-(\mu_B+N)}(\mu_B+N)^n}{n!} \Bigg/ \sum_{n=0}^{n_0} \frac{e^{-\mu_B}\mu_B^n}{n!} \tag{15}$$

This formalism yields "background subtracted" upper limits. It is applicable even when the expectation value for the background is larger than the observed number of events, since it takes background fluctuations properly into account. For $\mu_B = 0$ one recovers the usual equation without background subtraction.

A.3 Upper Limits with Background and Systematic Uncertainties

Systematic uncertainties are incorporated with the help of Gaussian smearing functions. Let σ_B be the uncertainty on the expected background μ_B, σ_S the *fractional* uncertainty on the expected signal μ_S, and define:

$$G(x;\mu,\sigma) = A(\mu,\sigma)\, e^{\frac{-(x-\mu)^2}{2\sigma^2}} \tag{16}$$

where A is a normalization factor:

$$A(\mu,\sigma) \int_0^{\infty} G(x;\mu,\sigma)\, dx \;=\; 1.0 \tag{17}$$

It is important to realize that this normalization condition defines A as a *function* of μ and σ. Upper limits are obtained by solving the following equation for N:

$$1 - \mathrm{CL} = \frac{\int_0^{\infty} dx\, G(x;\mu_B,\sigma_B) \int_0^{\infty} dy\, G(y;N,N\sigma_S) \sum_{n=0}^{n_0} \frac{e^{-(x+y)}(x+y)^n}{n!}}{\int_0^{\infty} dx\, G(x;\mu_B,\sigma_B) \sum_{n=0}^{n_0} \frac{e^{-x}x^n}{n!}} \tag{18}$$

We have assumed that uncertainties on signal and background are uncorrelated.

References

[1] F. Abe *et al.* Phy. Rev. D **45**, 3921 (1992).
"Limit on the top-quark mass from proton-antiproton collisions at $\sqrt{s} = 1.8$ TeV."

[2] T. Liss, CDF Note # 2367 (1993).
"High P_T CMU/CMP Muon Trigger Efficiencies for Run 1A"

[3] S. Kopp, CDF Note # 2391 (1993).
" Measurement of the Central Inclusive Electron Trigger Efficiency for the 1992-1993 Run 1A "

[4] We used efficiencies for PEM20 provided by A. Gordon early in the Run; his results are in very good agreement with an independent study by M. Dickson, CDF Note # 2147 (1993).
"Preliminary Measurement of Charge Asymmetry in W decays "

[5] CDF Note # 2245 (1993).
Sof Lepton Tag analysis.

[6] CDF Note # 2230 (1993).
SVX Tag analysis.

[7] A. Martin, CDF Note # 2230 (1993).
"Geometrical and kinematic acceptance of the leptons for top dilepton search."

[8] F. Abe *et al.* Phy. Rev. D **44**, 29 (1991).
"Measurement of $\sigma B(W \rightarrow e\nu)$ and $\sigma B(Z^0 \rightarrow e^+e^-)$ in proton-antiproton collisions at $\sqrt{s} = 1.8$ TeV."

[9] J. Wang and M. Contreras, CDF Note # 2108 (1993).
"Estimate of $Z^0 \rightarrow \tau^+\tau^-$ background in the Top Dilepton Analysis"

[10] J. Ohnemus, Phys. Rev. D **44**, 1403 (1991).

[11] M. Contreras and J. Wang, CDF Note # 2261 (1993).
"Estimate of the Drell-Yan Background in the Top Dilepton Analysis"

[12] L. Song, G. P. Yeh, and Q. F. Wang, CDF Note # 2106 (1993).
"Study of Top Dilepton Background from $b\bar{b}$ Sources"

[13] J. Romano and M. Contreras, CDF Note # 2107 (1993).
"Background due to Hadron Misidentification in the top Dilepton Search"

[14] Q. F. Wang, CDF Note # 2102 (1993).
" A Dilepton Fake Rate Study in Top Search"

[15] S. Kopp, CDF Note# 2218 (1993).
"The Fraction of High P_T Central Inclusive Electrons from b Quarks in Hadronic Jet Events"

[16] F. Abe *et al.* Phy. Rev. D **44**, 29 (1991).
"Measurement of $\sigma B(W \to e\nu)$ and $\sigma B(Z^0 \to e^+e^-)$ in $\overline{p}p$ collisions at $\sqrt{s} = 1800$ GeV."

[17] P. Nason, S. Dawson, and R. K. Ellis, Nucl. Phys. **B303**, 607 (1988).

[18] G. Altarelli, M. Diemoz, G. Martinelli, and P. Nason Nucl. Phys. **B308**, 724 (1988).

[19] R.K. Ellis, Phys. Lett. **B259**, 492 (1991).

[20] E. Laenen, J. Smith and W. van Neerven, Fermilab-Pub-93/270-T, (1993).

[21] G. Zech, "Upper limits in experiments with background or measurement uncertainties", Nucl. Instr. and Meth. **A277**, 608 (1989).

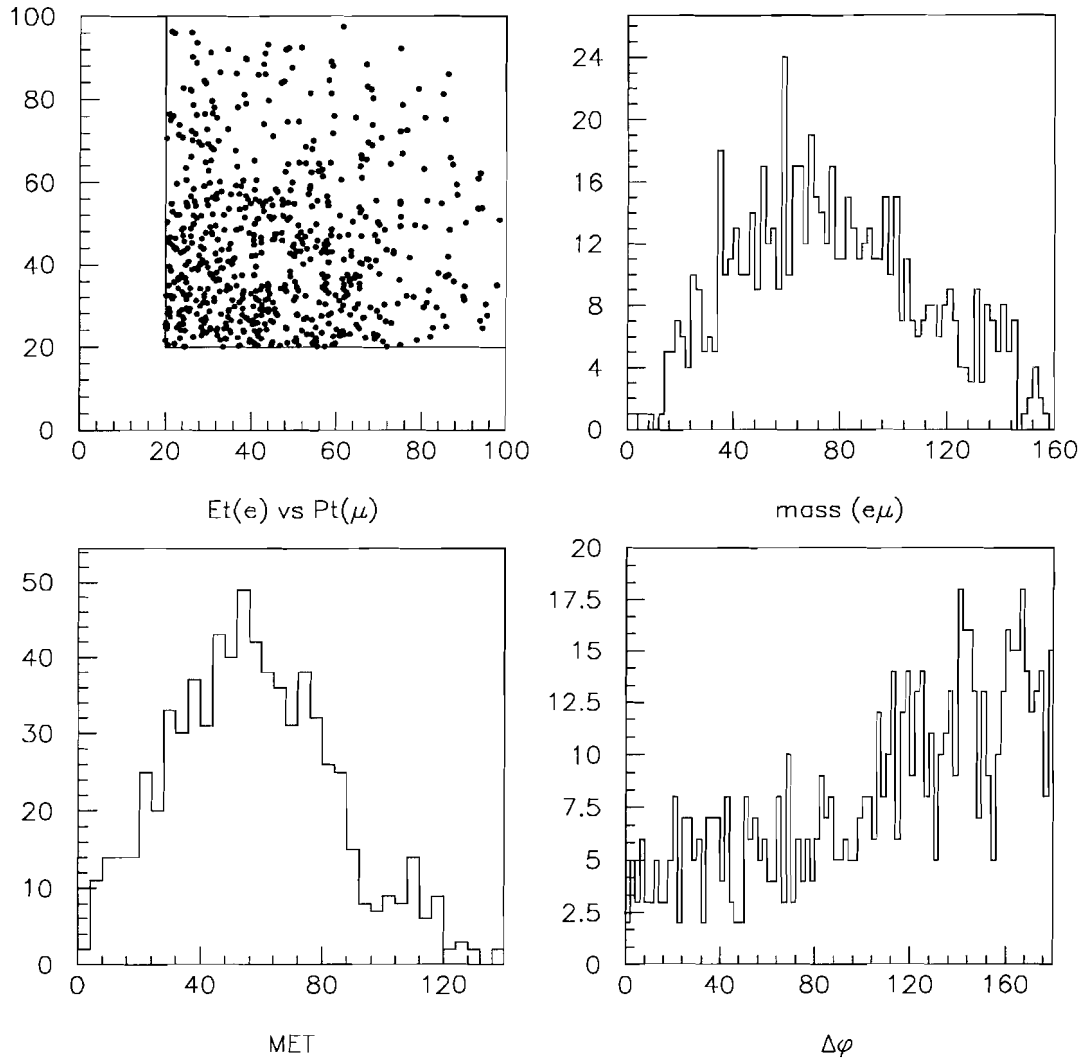

Figure : 1. Distributions of several reconstructed variables from Monte Carlo top events, for $M_{top} = 140$ GeV.
a) E_T(e) vs $P_T(\mu)$
b) Dilepton invariant mass
c) Missing E_T
d) $\Delta\phi_{\ell\ell}$ An integrated luminosity of the sample is 6780 pb^{-1}.

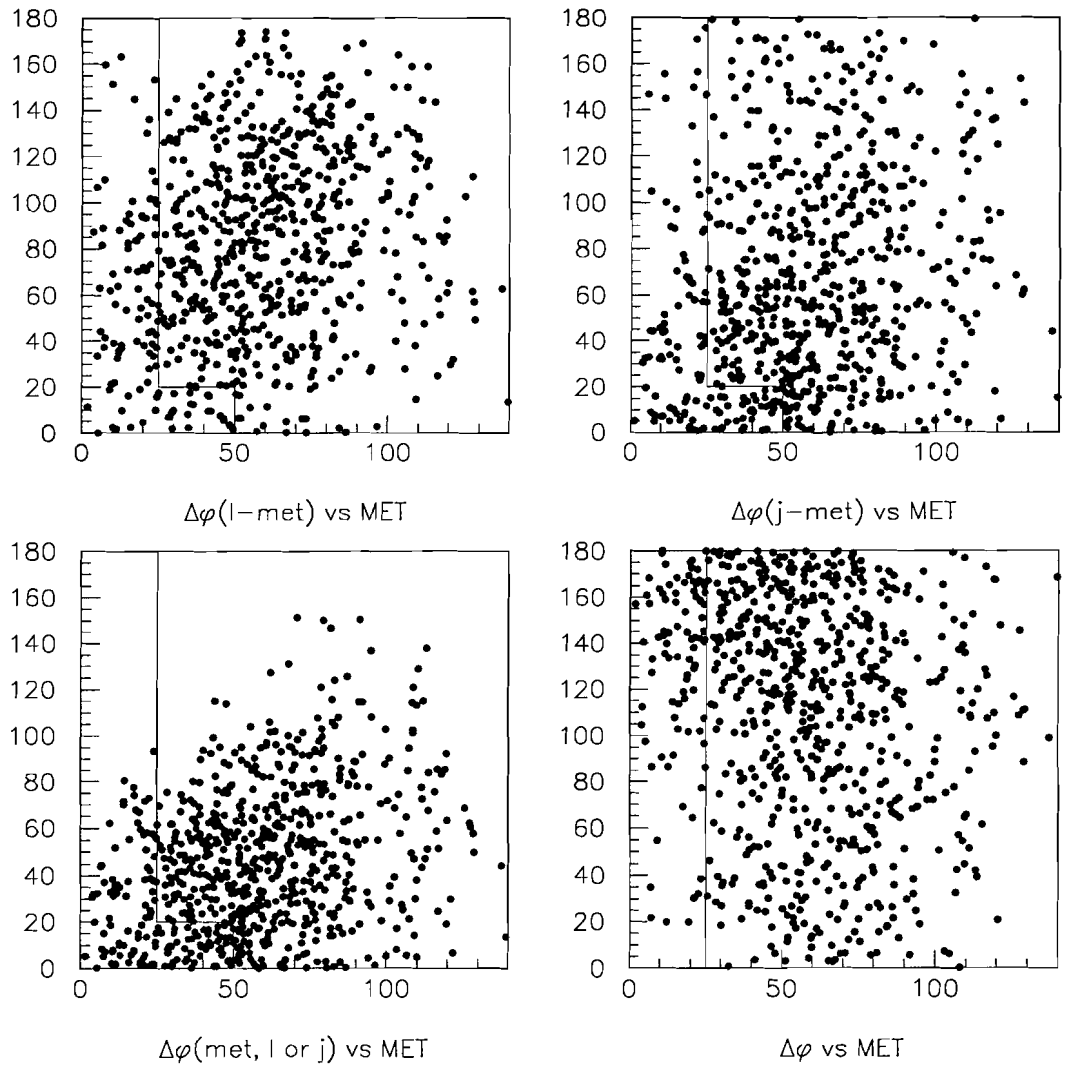

Figure : 1. Distributions of several reconstructed variables from Monte Carlo top events, for $M_{top} = 140$ GeV.
e) $\Delta\phi$ (Missing E_T,lepton) vs Missing E_T (only the closest lepton is plotted)
f) $\Delta\phi$ (Missing E_T,jet) vs Missing E_T (only the closest jet is plotted)
g) Min($\Delta\phi$ (Missing E_T, lepton), $\Delta\phi$ (Missing E_T, jet)) vs Missing E_T
h) $\Delta\phi_{\ell\ell}$ vs Missing E_T

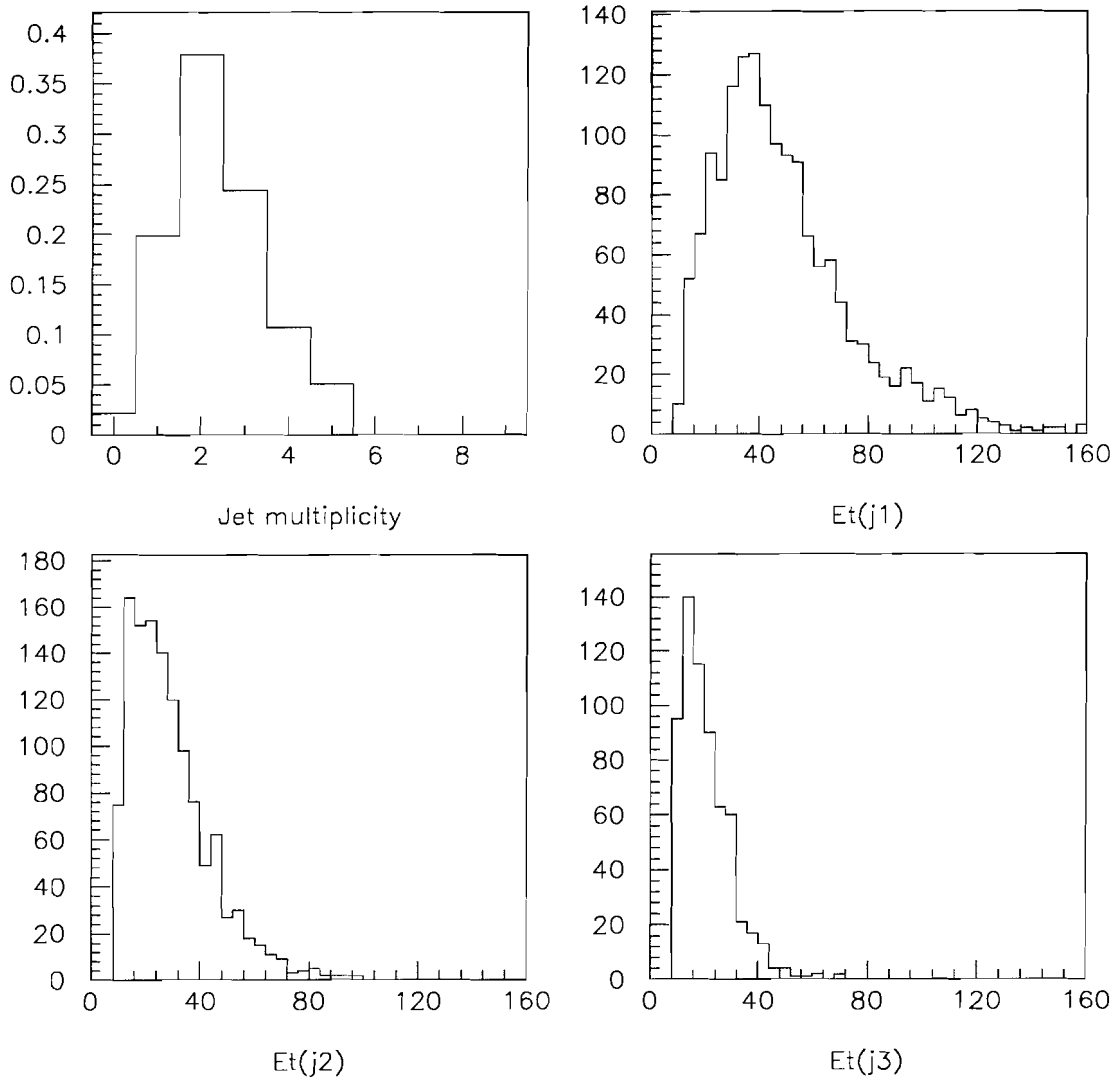

Figure : 1. Distributions of several reconstructed variables from Monte Carlo top events, for $M_{top} = 140$ GeV.
i) Jet multiplicity
j) E_T for Jet 1
k) E_T for Jet 2
l) E_T for Jet 3

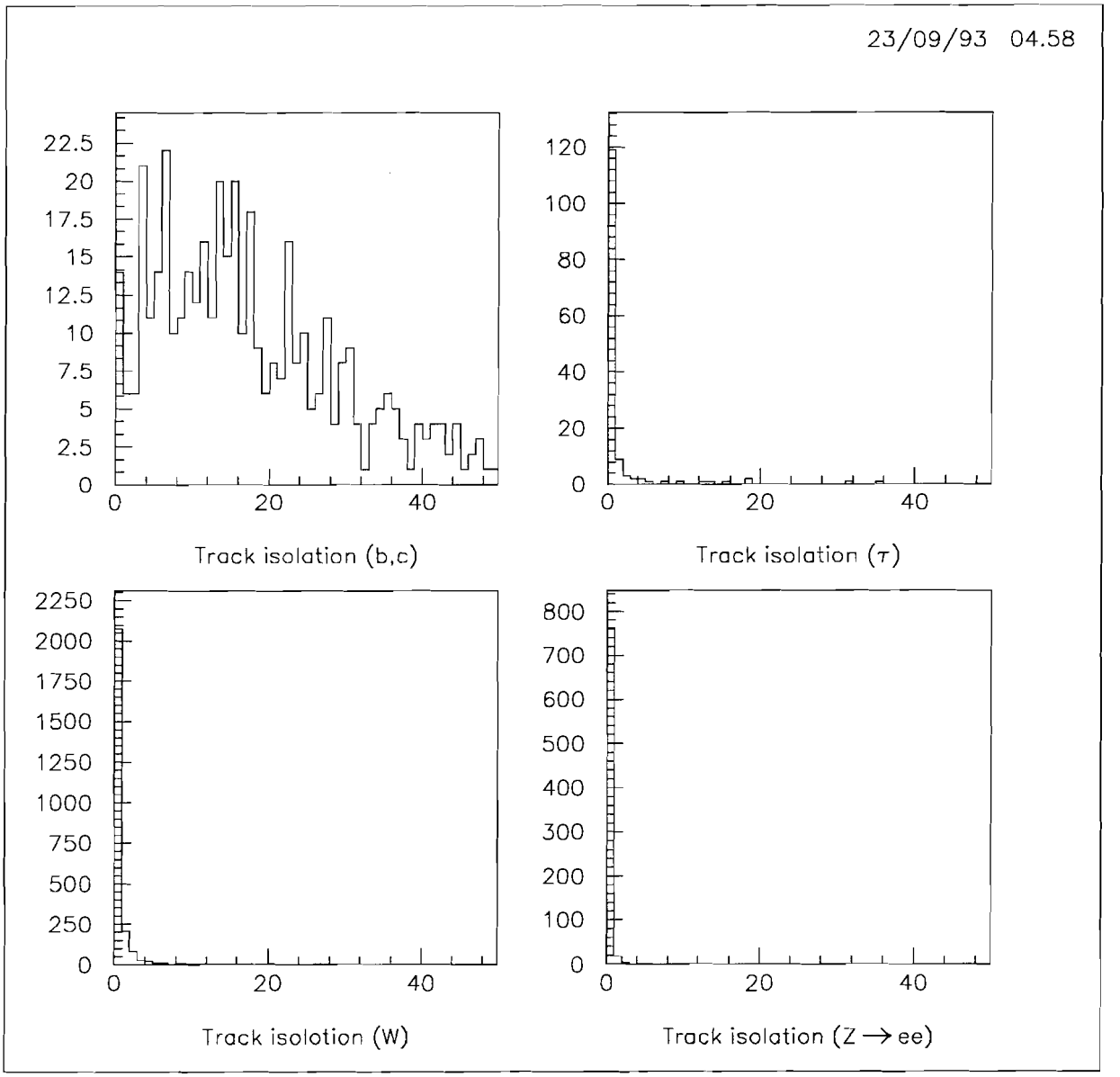

Figure : 2. Track isolation for electrons coming from:
a) (b,c) from top decay,
b) τ from top decay,
c) W from top decay, and
d) data $Z^0 \rightarrow$ ee.

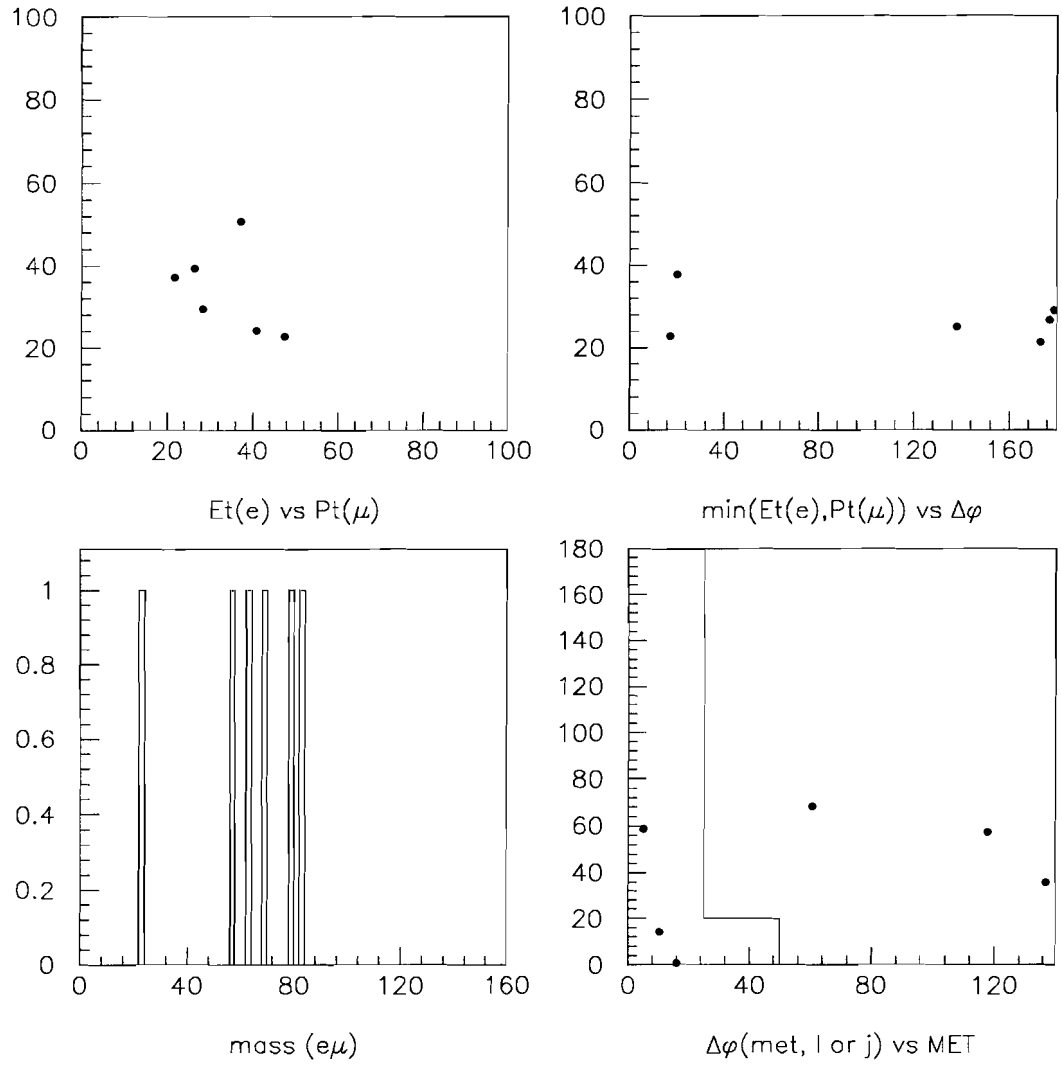

Figure : 3. Distributions for CDF $e\mu$ data for the complete 1992-93 run. There are two events in the signal region. All plots include the Pseudo-E Mu event (see text).
a) E_T(e) vs $P_T(\mu)$
b) Min(E_T,P_T) vs $\Delta\phi_{\ell\ell}$
c) Dilepton invariant mass
d) Azimuthal angle between the Missing E_T direction and the closest jet or lepton, versus Missing E_T

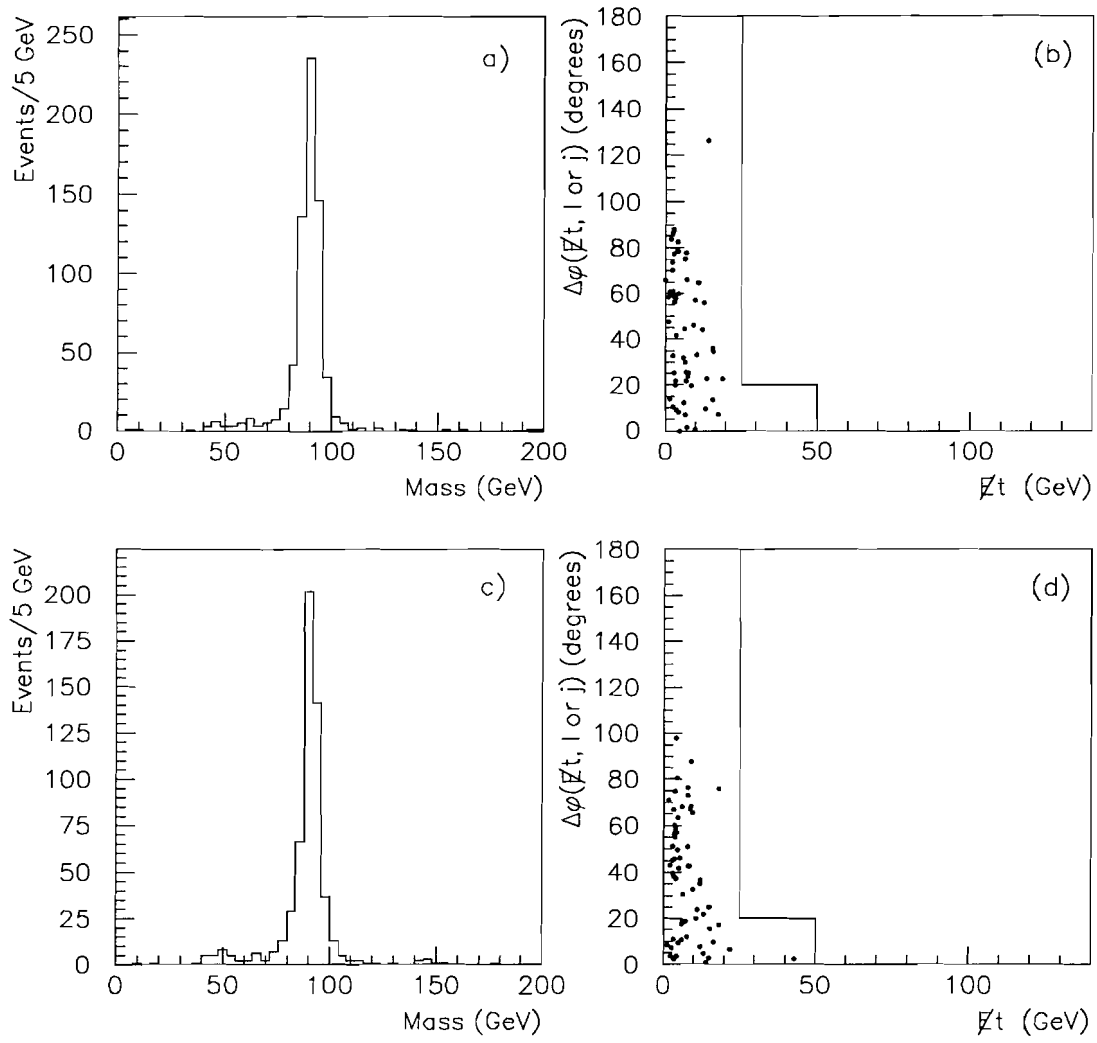

Figure : 4. Distributions for CDF data from the complete 1992-93 run. There are no dielectron or dimuon events in the signal region.
a) Dielectron invariant Mass
b) $\Delta\phi$ (Missing E_T, jet or lepton) vs missing E_T for dielectrons surviving the Z^0 mass window cut
c) Dimuon invariant Mass
d) $\Delta\phi$ (Missing E_T, jet or lepton) vs missing E_T for dimuons surviving the Z^0 mass window cut

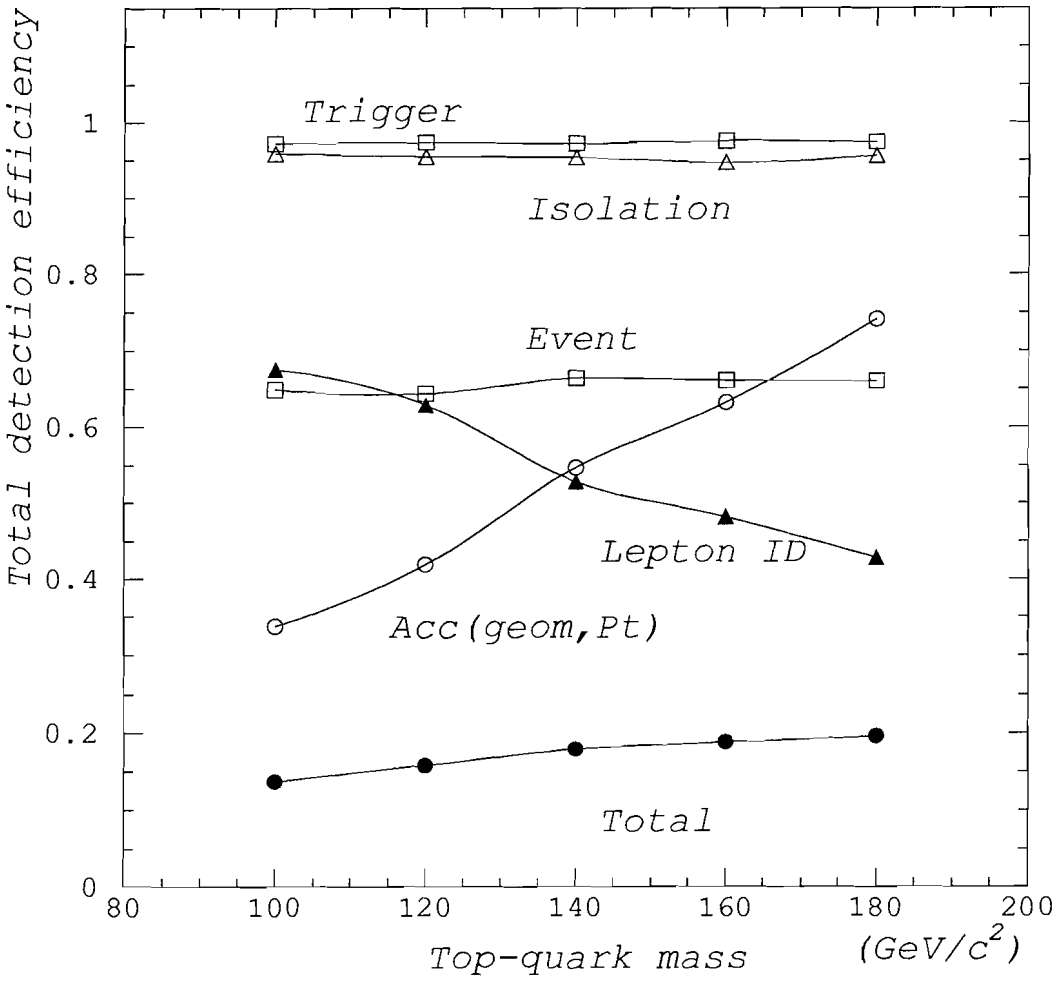

Figure : 5a. Efficiencies of the dilepton analysis as a function of M_{top} for the 92-93 run with standard cuts(no two jet cut) .

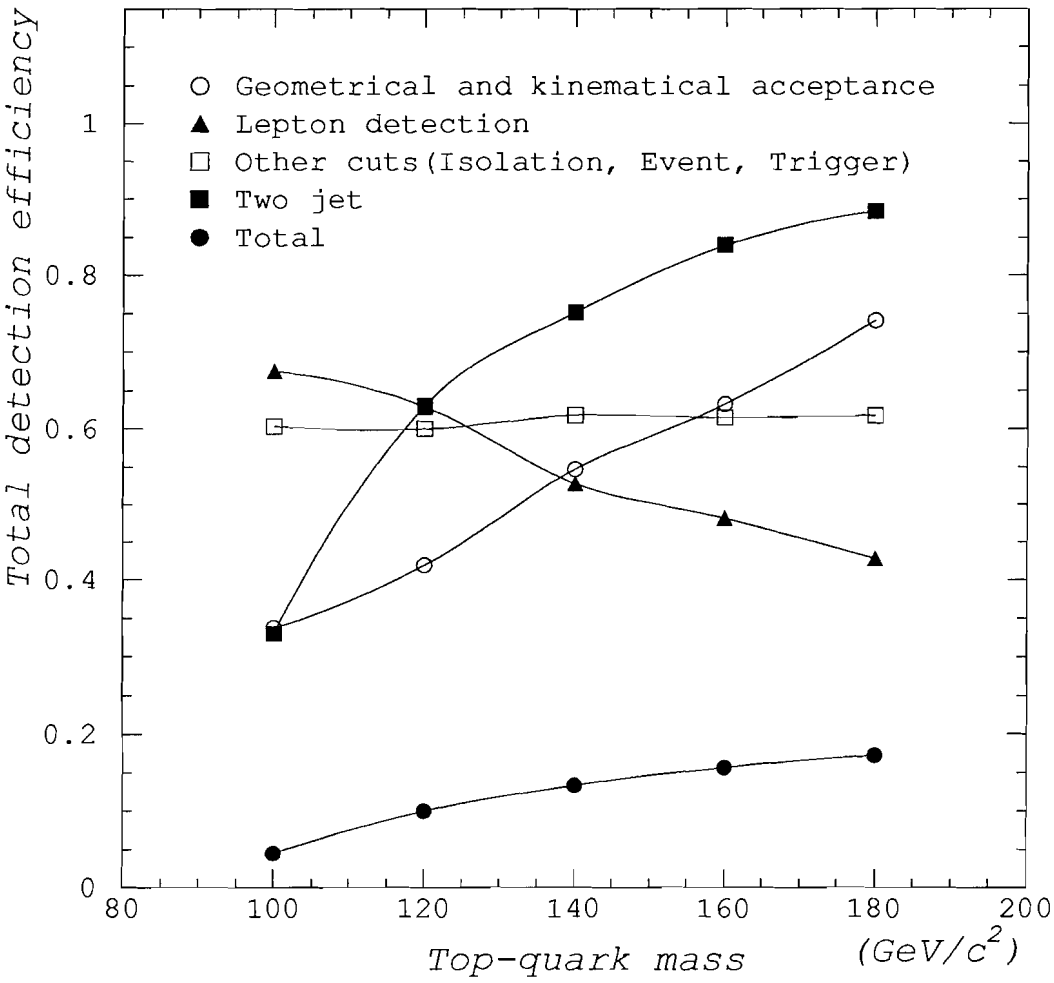

Figure : 5b. Efficiencies of the dilepton analysis as a function of M_{top}. for the 92-93 run with standard cuts + 2 jet cut.

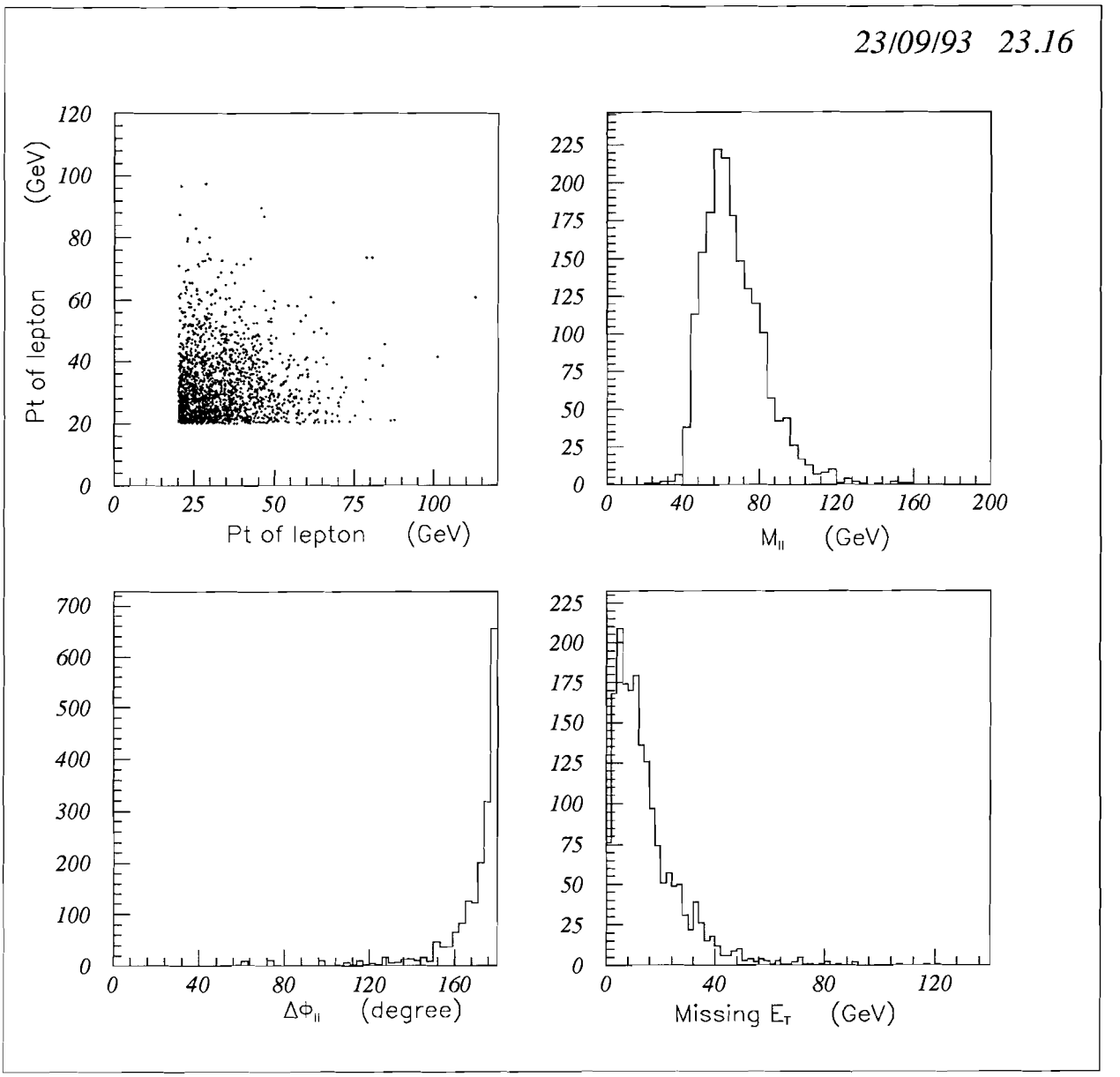

Figure : 6. Distributions of several reconstructed variables from $Z^0 \rightarrow \tau\tau$ Monte Carlo.
a) E_T(e) vs $P_T(\mu)$
b) Dilepton invariant mass
c) $\Delta\phi_{\ell\ell}$
d) Missing E_T

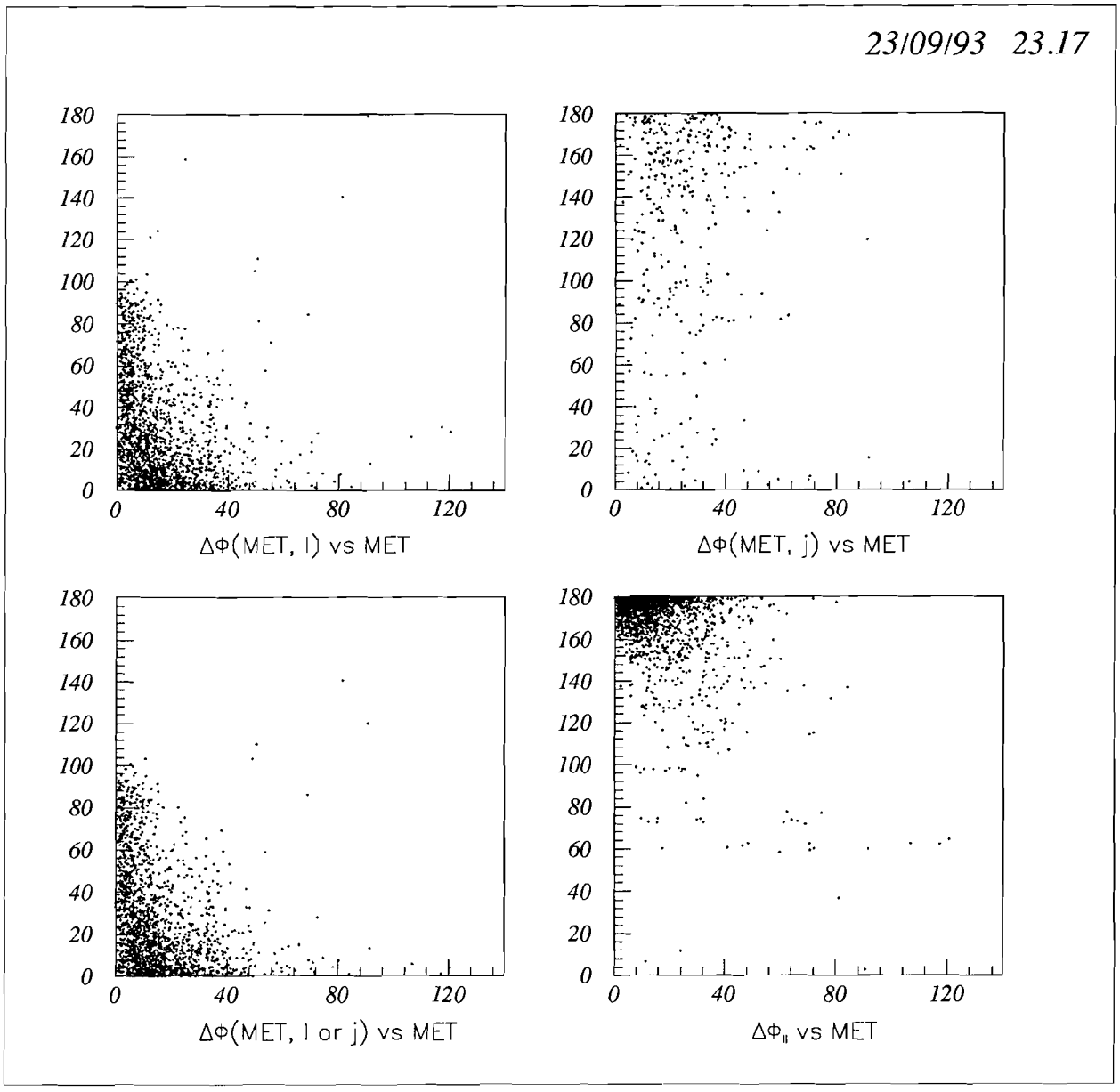

Figure : 6. Distributions of several reconstructed variables from $Z^0 \rightarrow \tau\tau$ Monte Carlo.
e) $\Delta\phi$ (Missing E_T,lepton) vs Missing E_T (only the closest lepton is plotted)
f) $\Delta\phi$ (Missing E_T,jet) vs Missing E_T (only the closest jet is plotted)
g) Min($\Delta\phi$ (Missing E_T, lepton), $\Delta\phi$ (Missing E_T, jet)) vs Missing E_T
h) $\Delta\phi_{\ell\ell}$ vs Missing E_T

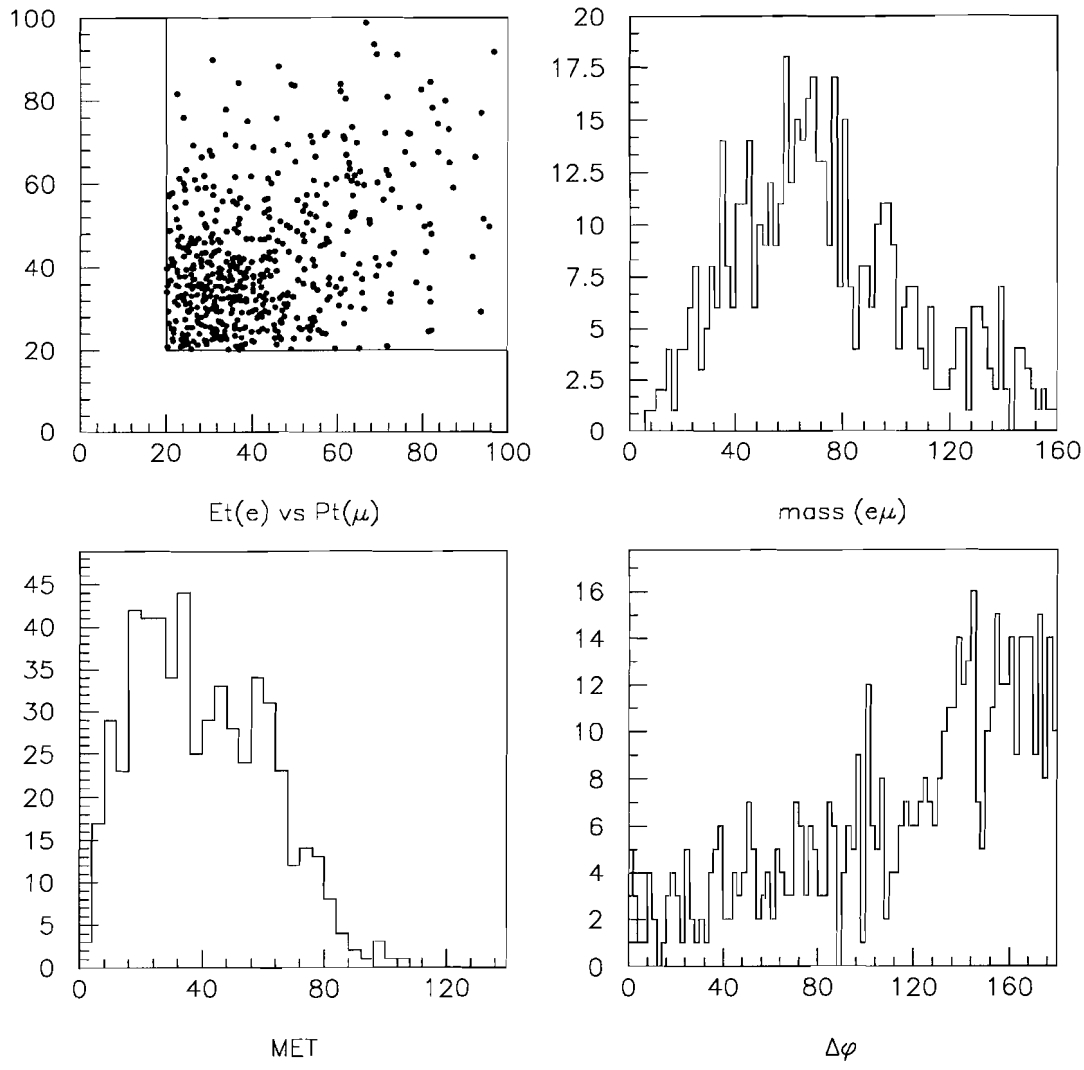

Figure : 7. Distributions of several reconstructed variables from WW Monte Carlo.
a) E_T(e) vs $P_T(\mu)$
b) Dilepton invariant mass
c) Missing E_T
d) $\Delta\phi_{\ell\ell}$

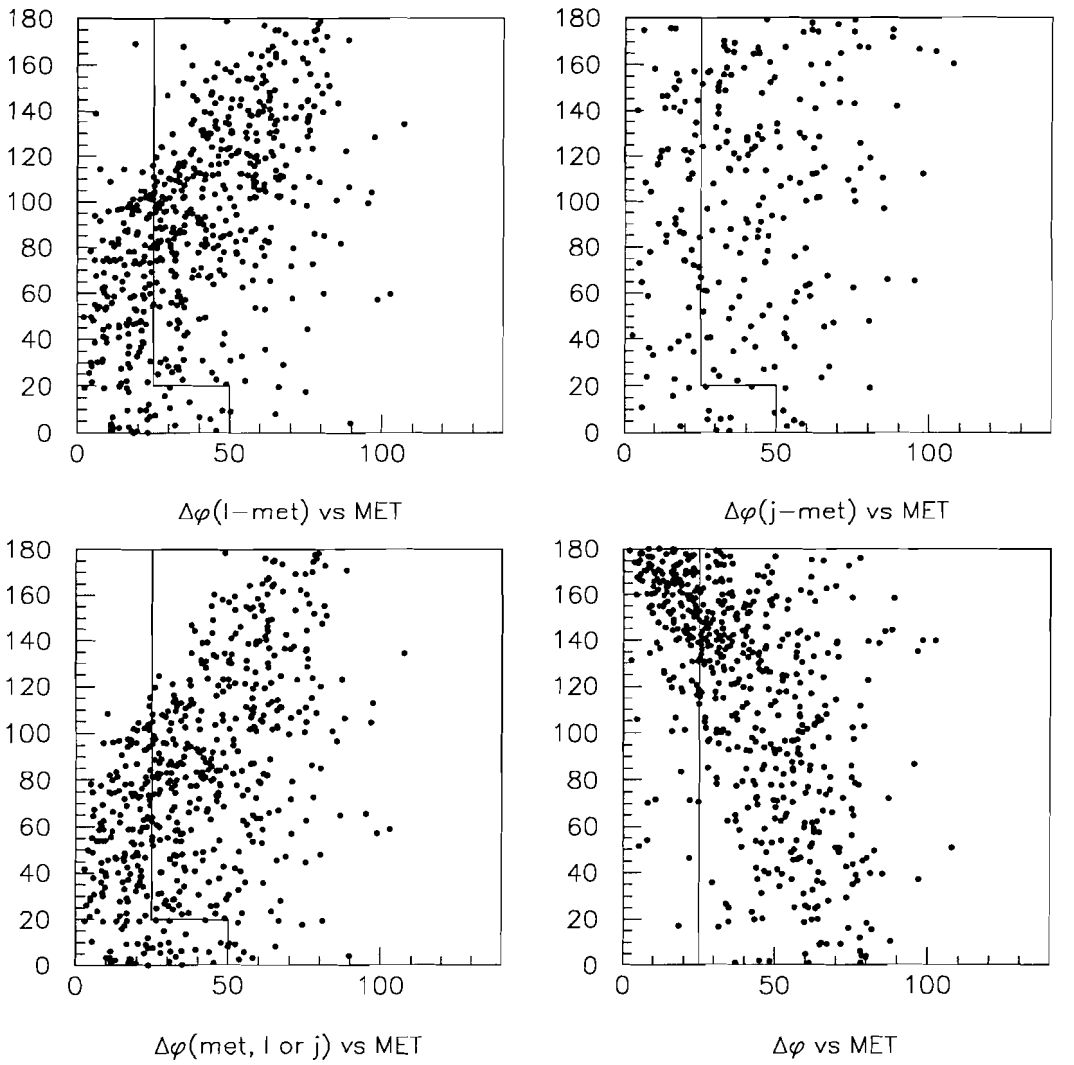

Figure : 7. Distributions of several reconstructed variables from WW Monte Carlo.
e) $\Delta\phi$ (Missing E_T,lepton) vs Missing E_T (only the closest lepton is plotted)
f) $\Delta\phi$ (Missing E_T,jet) vs Missing E_T (only the closest jet is plotted)
g) Min($\Delta\phi$ (Missing E_T, lepton), $\Delta\phi$ (Missing E_T, jet)) vs Missing E_T
h) $\Delta\phi_{\ell\ell}$ vs Missing E_T

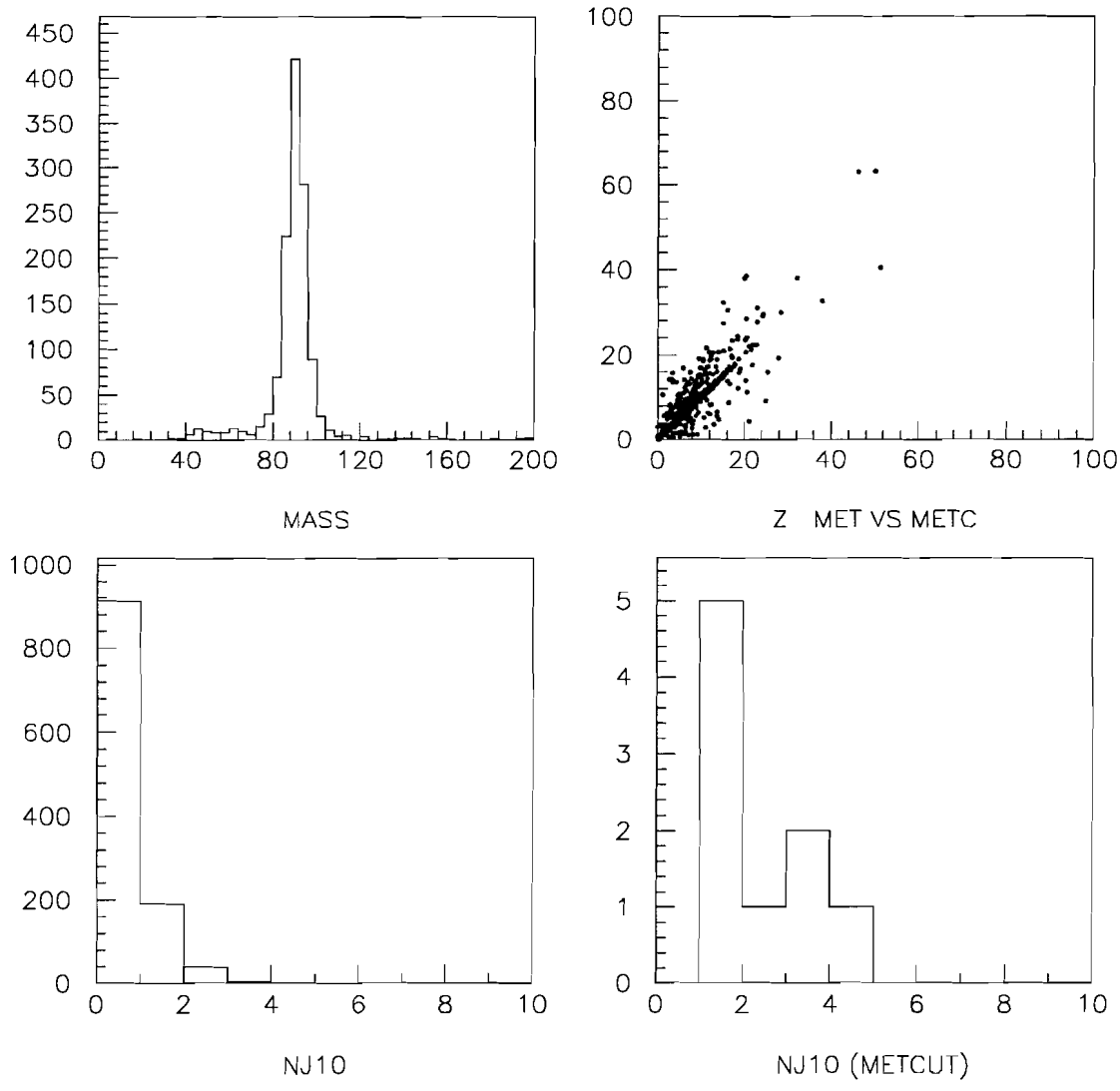

Figure : 8. CDF Z events from the 1992-93 run.
a) Dielectron and dimuon invariant mass distribution ($P_T > 20$ GeV/c).
b) Raw missing E_T versus corrected missing E_T; note that for large missing E_T the corrected quantity has better background rejection.
c) Number of jets with ET greater than 10 GeV.
d) Number of jets for events with corrected missing $E_T > 25$ GeV.

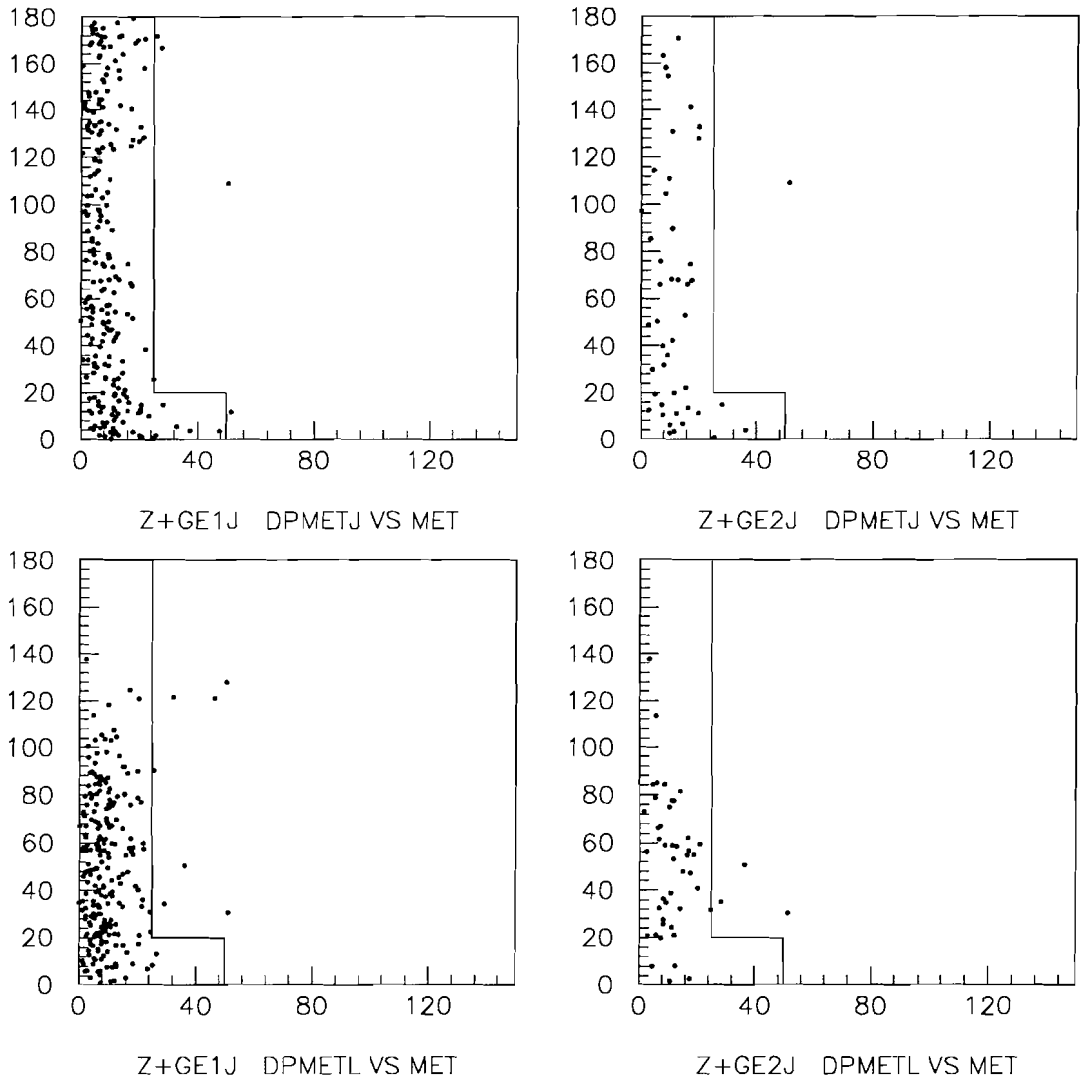

Figure : 8. CDF Z events from the 1992-93 run.
e) Azimuthal angle between the missing E_T direction and the closest jet, versus missing E_T, for Z events with at least one jet.
f) Azimuthal angle between the missing E_T direction and the closest jet, versus missing E_T, for Z events with at least two jets.
g) Azimuthal angle between the missing E_T direction and the closest lepton, versus missing E_T, for Z events with at least one jet.
h) Azimuthal angle between the missing E_T direction and the closest lepton, versus missing E_T, for Z events with at least two jets.

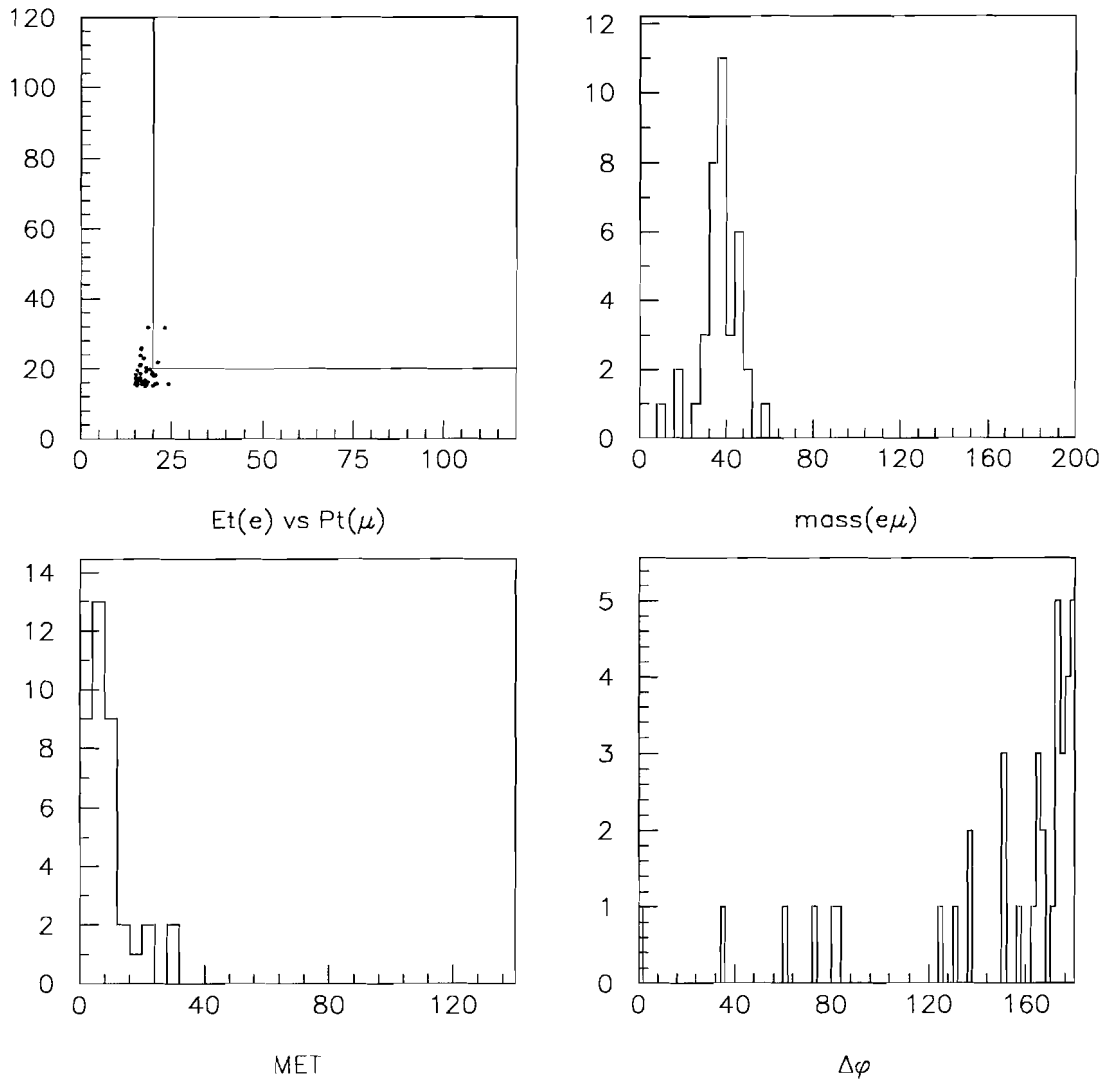

Figure : 9. Distributions of several reconstructed variables from $b\bar{b}$ Monte Carlo.
a) E_T(e) vs $P_T(\mu)$
b) Dilepton invariant mass
c) Missing E_T
d) $\Delta\phi_{\ell\ell}$

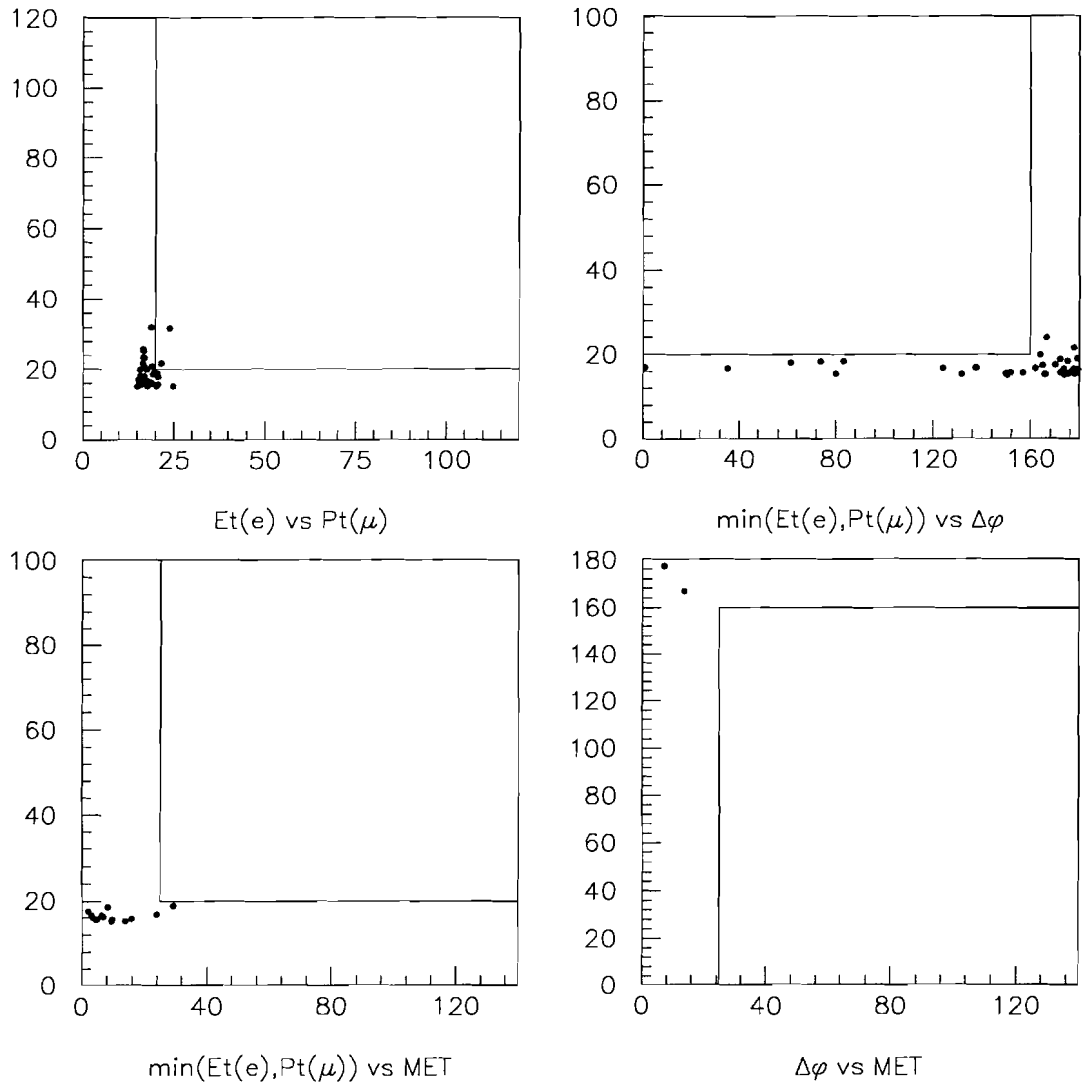

Figure : 9. Distributions of several reconstructed variables from $b\bar{b}$ Monte Carlo.
e) $E_T(e)$ vs $P_T(\mu)$
f) Min(E_T,P_T) vs $\Delta\phi_{\ell\ell}$
g) Min(E_T,P_T) vs Missing E_T
h) $\Delta\phi_{\ell\ell}$ vs Missing E_T

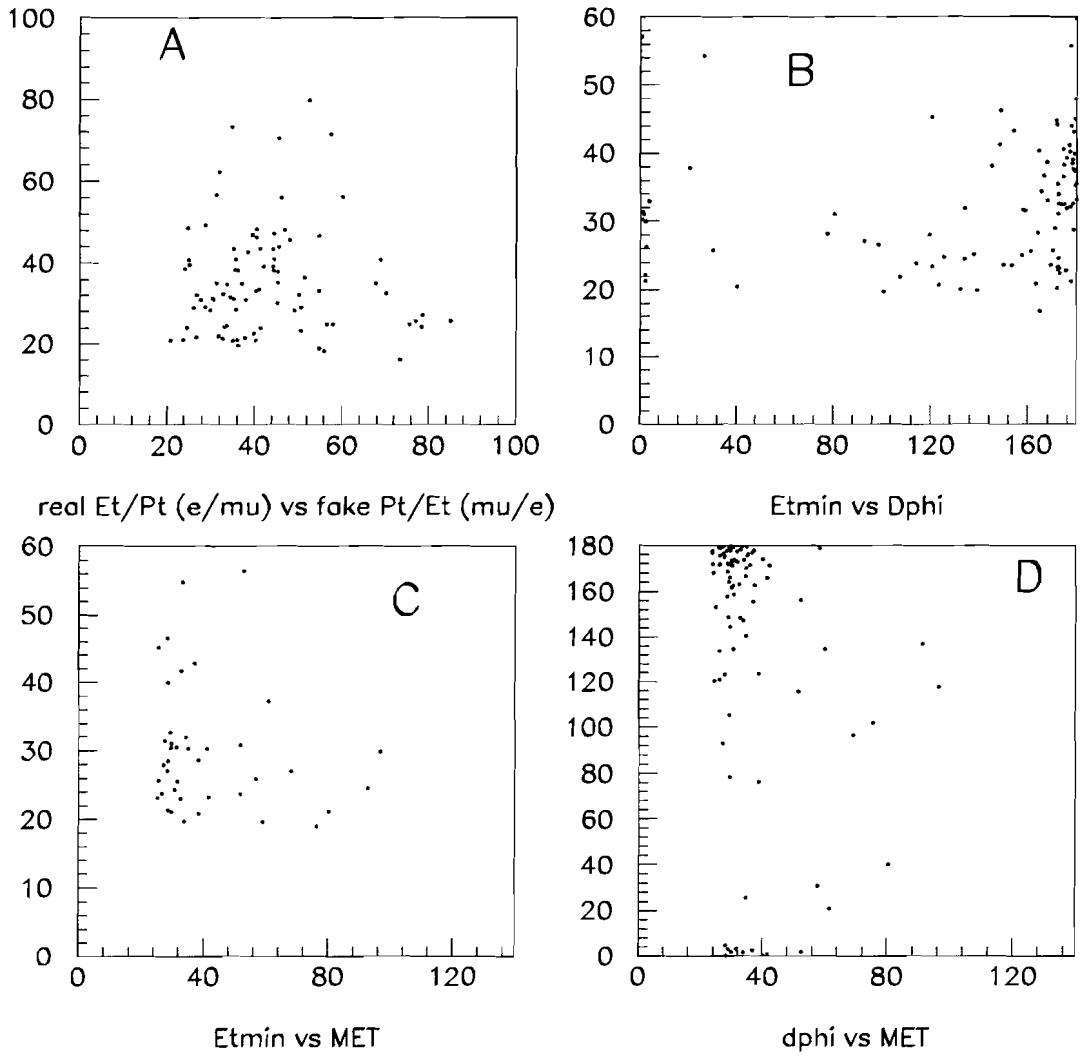

Figure : 10. Distributions of several reconstructed variables from the fake sample.
a) Real electron E_T(e) vs fake muon $P_T(\mu)$
b) Min(E_T,P_T) vs $\Delta\phi_{\ell\ell}$
c) Min(E_T,P_T) vs Missing E_T
d) $\Delta\phi_{\ell\ell}$ vs Missing E_T

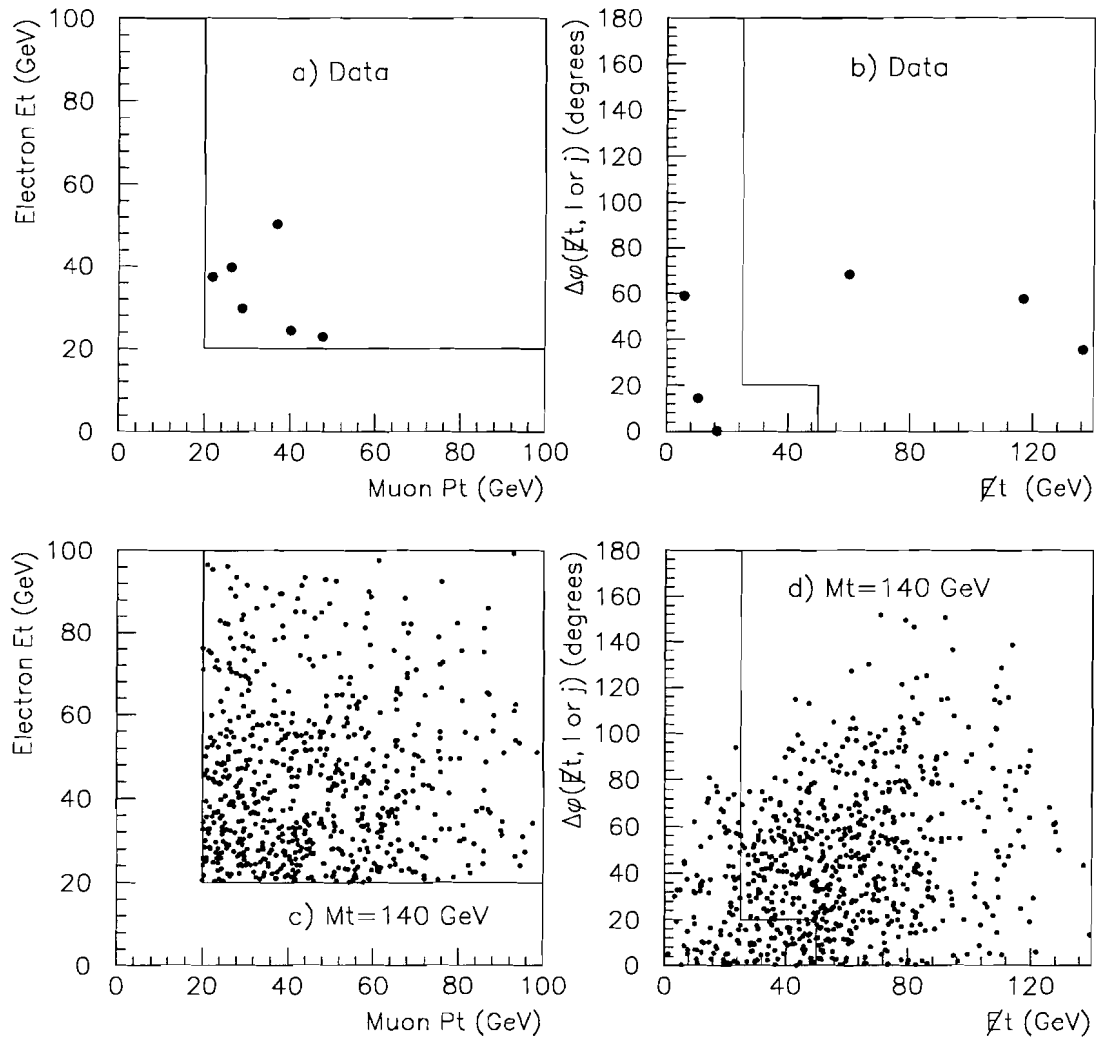

Figure : 11. Data versus Monte Carlo: $e\mu$ events.
a) $E_T(e)$ vs $P_T(\mu)$ (CDF 1992-93 data)
b) Min($\Delta\phi(\not\!\!E_T, \ell)$,$\Delta\phi(\not\!\!E_T, j)$) vs Missing E_T (CDF 1992-93 data)
There are two $e\mu$ events in the signal region. Plots a) and b) both include the Pseudo-E Mu event.
c) $E_T(e)$ vs $P_T(\mu)$ (Monte Carlo $t\bar{t}$ events with $M_{top} = 140$ GeV/c^2).
d) Min($\Delta\phi(\not\!\!E_T, \ell)$,$\Delta\phi(\not\!\!E_T, j)$) vs Missing E_T (Monte Carlo $t\bar{t}$ events with $M_{top} = 140$ GeV/c^2).

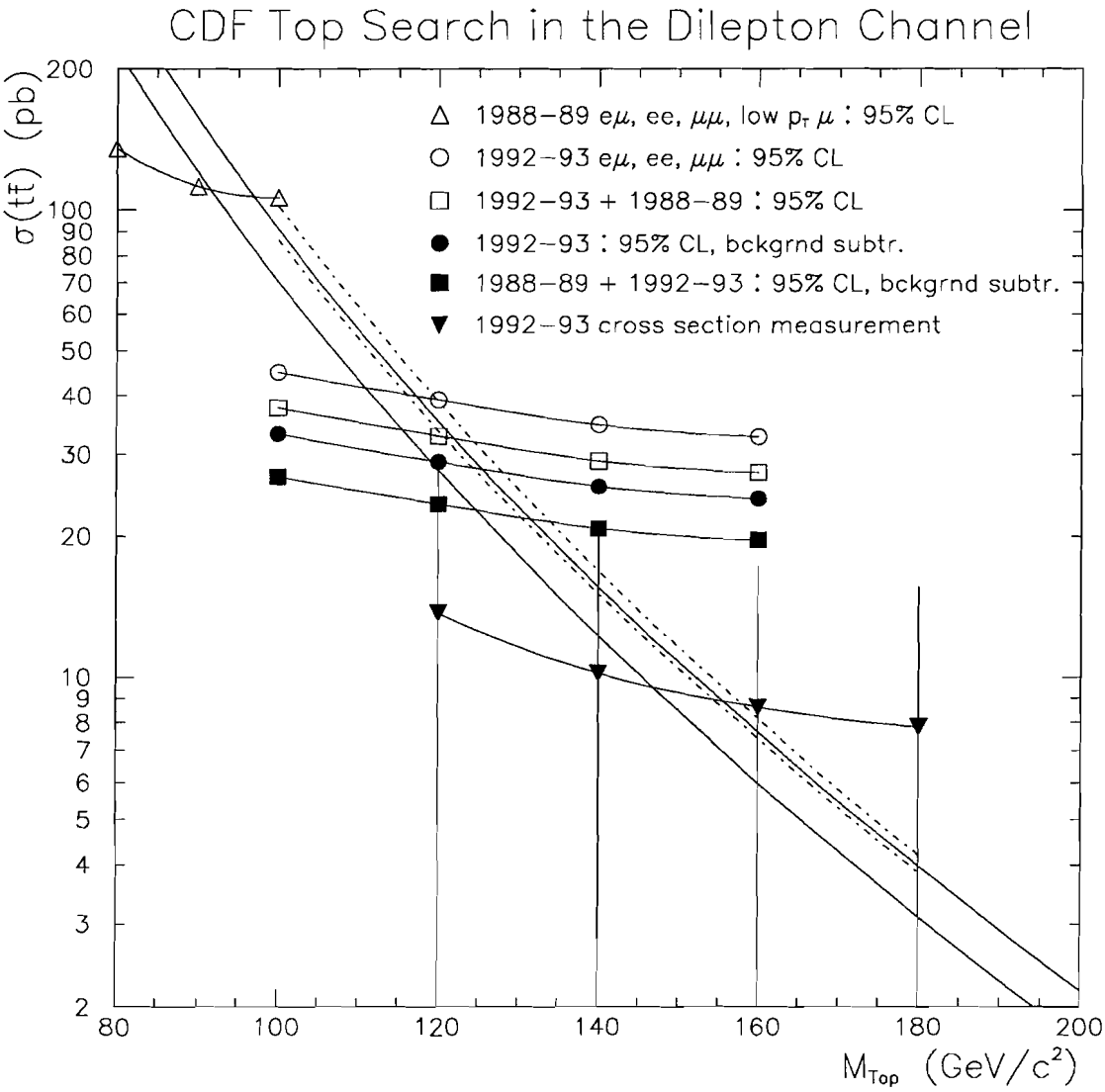

Figure : 12. $\sigma_{t\bar{t}}$ as a function of M_{top}; two theoretical calculations are shown, as well as an experimental measurement and several experimental upper limits; see text for a full description